TARGET GLINT PHENOMENON ANALYSIS AND EVALUATION OF GLINT REDUCTION TECHNIQUES

A THESIS SUBMITTED TO
THE GRADUATE SCHOOL OF NATURAL AND APPLIED SCIENCES
OF
MIDDLE EAST TECHNICAL UNIVERSITY

BY

SELÇUK BAHTİYAR

IN PARTIAL FULFILLMENT OF THE REQUIREMENTS
FOR
THE DEGREE OF MASTER OF SCIENCE
IN
ELECTRICAL AND ELECTRONICS ENGINEERING

SEPTEMBER 2012

Approval of the thesis:

TARGET GLINT PHENOMENON ANALYSIS AND EVALUATION OF GLINT REDUCTION TECHNIQUES

submitted by **SELÇUK BAHTİYAR** in partial fulfillment of the requirements for the degree of **Master of Science in Electrical and Electronics Engineering Department, Middle East Technical University** by,

Prof. Dr. Canan Özgen _____
Dean, Graduate School of **Natural and Applied Sciences**

Prof. Dr. İsmet Erkmen _____
Head of Department, **Electrical and Electronics Engineering**

Prof. Dr. S. Sencer Koç _____
Supervisor, **Electrical and Electronics Engineering Dept., METU**

Examining Committee Members:

Prof. Dr. Yalçın Tanık _____
Electrical and Electronics Engineering Dept., METU

Prof. Dr. S. Sencer Koç _____
Electrical and Electronics Engineering Dept., METU

Assoc. Prof. Çağatay Candan _____
Electrical and Electronics Engineering Dept., METU

Assoc. Prof. Ali Özgür Yılmaz _____
Electrical and Electronics Engineering Dept., METU

Dr. Ülkü Çilek Doyuran _____
ASELSAN

Date: 12.09.2012

I hereby declare that all information in this document has been obtained and presented in accordance with academic rules and ethical conduct. I also declare that, as required by these rules and conduct, I have fully cited and referenced all material and results that are not original to this work.

Name, Last name: SELÇUK BAHTİYAR

Signature :

ABSTRACT

TARGET GLINT PHENOMENON ANALYSIS
AND
EVALUATION OF GLINT REDUCTION TECHNIQUES

Bahtiyar, Selçuk

M. S., Department of Electrical and Electronics Engineering

Supervisor: Prof. Dr. Sencer Koç

September 2012, 87 pages

In this thesis, target induced glint error phenomenon is analyzed and the glint reduction techniques are evaluated. Glint error reduction performance of the methods is given in a comparative manner.

First, target glint is illustrated with the dumbbell model which has two point scatterers. This illustration of the glint error builds the basic notion of target scattering centers and effect of scattering characteristics on glint error. This simplest approach is also used to understand the glint reduction methods.

In an effort to evaluate the glint reduction techniques, a model based upon the concept of coherent summation of scattering complexes is used. The model is also used for introducing the basic properties of glint phenomenon.

Basics of the glint phenomenon and glint reduction techniques are discussed with particular emphasis on diversity methods. Frequency diversity and spatial diversity techniques are described and investigated with generated simulation data. The diversity selection methods which are used to eliminate the erroneous data are introduced and their performances are investigated.

Glint error reduction results of various scenarios including both reduction techniques and selection methods are evaluated in comparison with each other. The results indicate that significant reduction of glint error is possible by the appropriate utilization of diversity techniques in radar systems.

Keywords: Target Glint, Dumbbell Model, Glint Reduction Techniques, Frequency Diversity, Spatial Diversity, Diversity Selection Methods

ÖZ

HEDEF PARILTI OLGUSU ANALİZİ
VE
PARILTI AZALTMA YÖNTEMLERİNİN DEĞERLENDİRİLMESİ

Bahtiyar, Selçuk

Yüksek Lisans, Elektrik ve Elektronik Mühendisliği Bölümü

Tez Yöneticisi: Prof. Dr. Sencer Koç

Eylül 2012, 87 sayfa

Bu tezde, hedef kaynaklı parıltı olgusu analizi ve parıltı azaltma yöntemlerinin değerlendirmesi yapılmıştır. Parıltı azaltma yöntemlerinin performansları karşılaştırmalı şekilde verilmiştir.

Öncelikli olarak üzerinde iki saçıcı bulunan dambıl modeli ile hedef parıltısı gösterimi yapılmıştır. Bu gösterim hedef saçıcı merkezleri olgusunun ve saçıcı karakteristiklerinin parıltı üzerine etkisinin temelini oluşturmaktadır. En basit haliyle parıltının bu gösterimi, parıltı azaltma yöntemlerinin anlaşılması için de kullanılmıştır.

Parıltı azaltma yöntemlerinin değerlendirilmesi amacıyla, saçıcı etkilerinin eşevreli bir araya getirilmesi üzerine kurulu bir model kullanılmıştır. Bu model parıltı olgusunun temel özelliklerini göstermek amacıyla da kullanılmıştır.

Parıltı olgusunun temelleri ve parıltı azaltma yöntemleri çeşitlilik yaratma yöntemlerine vurgu yaparak açıklanmıştır. Frekans çeşitliliği ve uzaysal çeşitlilik teknikleri açıklanmış ve üretilen benzetim verisiyle incelenmiştir. Hata içeren verileri ayıklamak amacıyla çeşitlilik seçim yöntemleri kullanılmıştır. Kullanılan yöntemler açıklanmış ve performansları incelenmiştir.

Çeşitlilik tekniklerini ve çeşitlilik seçim yöntemlerini içeren senaryoların parıltı kaynaklı hata azaltma sonuçları birbirleriyle karşılaştırmalı olarak değerlendirilmiştir. Sonuçlar, radar sistemlerinde çeşitlilik tekniklerinin uygun kullanımlarının kayda değer parıltı hatası indirgemesi yapılabileceğini göstermektedir.

Anahtar Kelimeler: Hedef Parıltısı, Dambıl Modeli, Parıltı Azaltma Yöntemleri, Frekans Çeşitliliği, Uzaysal Çeşitlilik, Çeşitlilik Seçim Yöntemleri

To My Family

and

My Beloved Başak

ACKNOWLEDGMENTS

I would like to express my deepest gratitude to my supervisor Prof. Dr. Seyit Sencer Koç for his encouragements, guidance, advice, criticism and insight throughout the research.

I would like to thank ASELSAN Inc. for opportunities provided for the completion of this thesis. I am also grateful to my colleagues for their support.

I would also like to thank my Mom, Kadriye Bahtiyar, my brother Serhan Yılmaz, my grandparents, Behiye and Yusuf Bahtiyar and my uncle Bedri Bahtiyar for their endless support and trust not only throughout my thesis but also throughout my life.

Last but not least, I am grateful to my fiancée, Başak Gümüştekin, for her love and every moment for years and years to come.

TABLE OF CONTENTS

ABSTRACT iv

ÖZ vi

ACKNOWLEDGMENTS viii

TABLE OF CONTENTS x

LIST OF TABLES xii

LIST OF FIGURES xiii

CHAPTERS

1. INTRODUCTION 1

1.1. Introduction 1
1.2. Motivation 4
1.3. Thesis Objectives 4
1.4. Outline of the Thesis 5

2. TWO POINT TARGET GLINT ILLUSTRATION 6

2.1. Two Point Target 6
2.2. Basic Glint Relations of Two Point Target 7

3. GLINT BACKGROUND AND SIMULATION MODEL 14

3.1. Direction Finding 14
3.1.1. Monopulse Techniques 15
3.1.1.1. Amplitude Comparison Monopulse 16
3.1.1.2. Phase Comparison Monopulse 17
3.2. Prior Glint Investigation 18
3.3. Glint Simulation Model 21
3.3.1. N-Point Scattering Element Geometry 22
3.3.2. Generating Target Return Signal 23
3.3.2.1. Return Signal With Different Antennas 24
3.3.2.2. Return Signal With Different Transmit/Receive Patterns 25
3.3.3. Target Angle Estimation 26
3.3.3.1. Comparison of DF Methods 28

4. GLINT PROPERTIES AND REDUCTION METHODS 30
4.1. INTRODUCTION 30
4.2. GLINT PROPERTIES 30
4.2.1. The relationship between glint and target range 31
4.2.2. The relationship between glint and echo amplitude 34
4.2.3. The relationship between glint and target size 36
4.2.4. Evaluation of Glint Properties 38
4.3. GLINT REDUCTION TECHNIQUES 39
4.3.1. Diversity Selection Methods 42
5. GLINT REDUCTION ANALYSIS 46
5.1. FREQUENCY DIVERSITY 46
5.1.1. Autocorrelation Function of Frequency Agile Signals 47
5.1.2. Critical Frequency Change 50
5.1.3. Improvement with Frequency Agility 51
5.1.4. Simulation Results of Frequency Agility 53
5.1.4.1. Effect of Sample Number in a Fixed Bandwidth 53
5.1.4.2. Effect of Agility Bandwidth for Fixed Number of Samples 59
5.1.4.3. Frequency Spacing Regime Effect on Reduction 64
5.2. SPATIAL DIVERSITY 66
5.2.1. Autocorrelation Function of Signals with Spatial Diversity 67
5.2.2. Critical Angle Change 69
5.2.3. Critical Antenna Movement 70
5.2.4. Improvement with Spatial Diversity 71
5.2.5. Simulation Results of Spatial Diversity 73
5.2.5.1. Effect of Sample Number for a Fixed Spatial Shift 73
5.2.5.2. Effect of Spatial Shift for a Fixed Number of Samples 77
5.2.5.3. ISAR like Reduction Results 80
6. CONCLUSION 83
REFERENCES 85

LIST OF TABLES

TABLES

Table 3.1 Simulation configuration of DF methods comparison analysis 27
Table 4.1 Simulation configuration of range effect analysis 31
Table 4.2 Simulation configuration of amplitude-glint correlation analysis 34
Table 4.3 Simulation configuration of target size effect on glint analysis 36
Table 4.4 Simulation configuration of diversity selection method analysis 42
Table 5.1 Approximate improvement with frequency diversity 51
Table 5.2 Simulation configuration of sample number analysis 52
Table 5.3 Simulation configuration of frequency agility bandwidth analysis 57
Table 5.4 Simulation configuration of sample spacing regime 62
Table 5.5 Simulation configuration of sample number analysis 71
Table 5.6 Simulation configuration of antenna movement analysis 76
Table 5.7 Simulation configuration of ISAR like reduction 79

LIST OF FIGURES

FIGURES

Figure 1.1 General block diagram of radar 2
Figure 2.1 Target geometry for dumbbell model 6
Figure 2.2 Apparent center shift of two point target 9
Figure 2.3 Normalized error factor for two point target 12
Figure 3.1 Amplitude monopulse antenna pattern 16
Figure 3.2 The beam patterns, sum and difference patterns and the difference to sum ratio 16
Figure 3.3 Phase comparison monopulse geometry 17
Figure 3.4 General target and radar geometry for simulation 22
Figure 3.5 Comparison of DF methods 28
Figure 4.1 Average target range effect simulation results 32
Figure 4.2 Single run target range effect simulation results 32
Figure 4.3 Scatter-plot of echo amplitude and absolute angular error results 34
Figure 4.4 Angular glint errors and corresponding echo amplitude values 35
Figure 4.5 Average target size effect simulation result 37
Figure 4.6 Single run target size effect simulation result 37
Figure 4.7 Angular glint error for different frequencies and aspects 40
Figure 4.8 Glint error reduction with selection methods 43
Figure 4.9 Mean glint error levels for different selection methods 43
Figure 5.1 Target geometry for autocorrelation function 46
Figure 5.2 Example of target signal's autocorrelation envelope for frequency change 48
Figure 5.3 Target 1 simulation results for 100MHz bandwidth 53
Figure 5.4 Target 1 simulation results for 500MHz bandwidth 54
Figure 5.5 Target 2 simulation results for 100MHz bandwidth 55
Figure 5.6 Target 2 simulation results for 500MHz bandwidth 56
Figure 5.7 Target 2 simulation results for 1000MHz bandwidth 56
Figure 5.8 Target 1 simulation results for 10 samples in bandwidth 58
Figure 5.9 Target 1 simulation results for 30 samples in bandwidth 59

Figure 5.10 Target 2 simulation results for 10 samples in bandwidth 60
Figure 5.11 Target 2 simulation results for 30 samples in bandwidth 61
Figure 5.12 Simulation results for 50 samples in bandwidth for target of 0.5m extending in range and crossrange 61
Figure 5.13 Sample number effect in both spacing regime 63
Figure 5.14 Frequency agility bandwidth effect for both spacing regime 63
Figure 5.15 Simple target geometry with aspect diversity 66
Figure 5.16 Example of target signal's autocorrelation envelope for aspect changes 68
Figure 5.17 Target 1 simulation results for 10m antenna movement 72
Figure 5.18 Target 1 simulation results for 40m antenna movement 73
Figure 5.19 Target 2 simulation results for 10m antenna movement 74
Figure 5.20 Target 2 simulation results for 40m antenna movement 74
Figure 5.21 Antenna movement effect on the reduction 77
Figure 5.22 Target geometry with rotating element 78
Figure 5.23 Glint reduction with the usage of target maneuver 79

CHAPTER 1

INTRODUCTION

1.1. Introduction

The word radar is an abbreviation for *RA*dio *D*etection *A*nd *R*anging. Radar is an electromagnetic sensor for detection of reflecting objects. Besides detecting the objects, it can also give information about its range, velocity, angular position and other identifying target characteristics. In addition, radars are also used for imaging of the terrain or the targets [1-3].

The history of radar starts with the experiments of Heinrich Hertz who showed that radio waves were reflected by metallic objects in the late 19^{th} century. However, it was German engineer Christian Huelsmeyer who first used them in order to build a simple radar that detects ships in fog for avoiding them to collide [4].

After this demonstration in 1904 by Huelsmeyer, the development of the radar is continued during World War II. The progress during the war was rapid and of great importance. After the war, the use of radar widened to various areas such as meteorology, speed guns for police, marine navigation.

The radar studies and enhancements are continued in many areas with different perspectives. Despite the complex structure of the radar, it can be simply considered as transmitting electromagnetic energy into a specified volume and processing the energy reflected by this volume (radar returns or echoes). The operation of a radar system can be summarized as [2]:

- The radar radiates electromagnetic energy from an antenna.
- Some of this energy is intercepted by an object or target.
- Target reradiates the intercepted energy to many directions.
- Some of this reradiated energy (echo) is received by the radar antenna.
- Received energy is amplified properly.
- Signal is processed to obtain information about the target with the help of signal processing algorithms.

The block diagram of a generic radar system is given in Figure 1.1, based on the above mentioned operations. The display of target is the output of the signal processing stage. Signal processing algorithms deal with various subjects in the extraction of target information. The problems which are related to target such as presence, velocity, angular bearing or movement direction are also handled by signal processing.

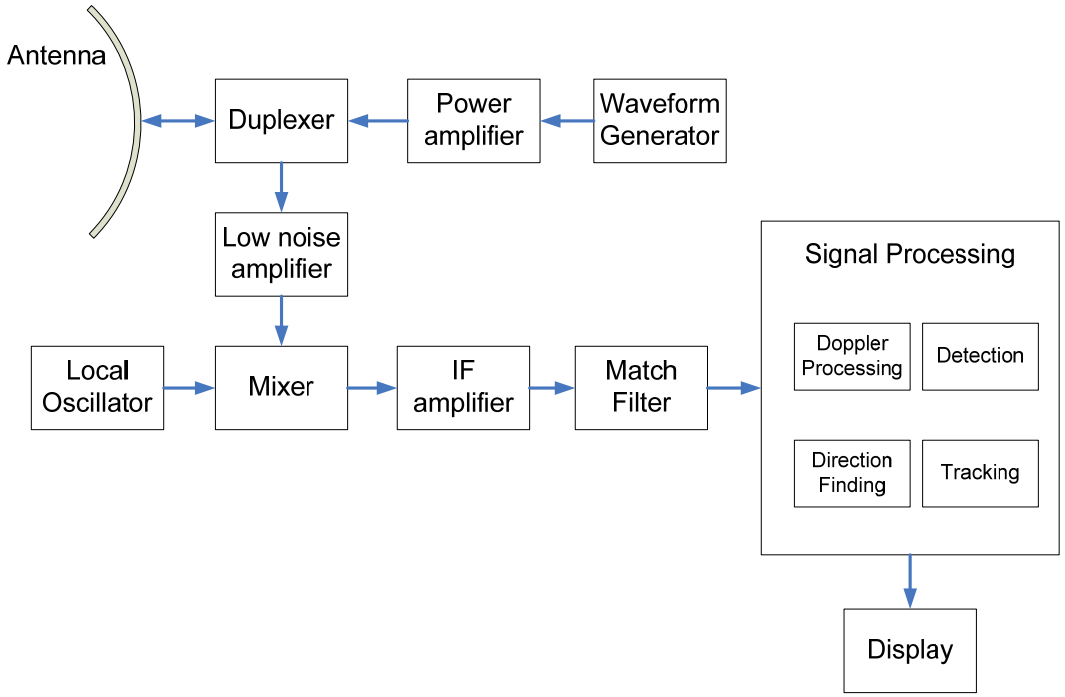

Figure 1.1 - General block diagram of radar

The error sources in the system may reduce the performance of the signal processing algorithms and cause inaccurate information about target. These errors can be originated from the radar itself, operating environment or target structure.

High precision tracking radar applications need to avoid the tracking errors for high performance. There are many error sources in tracking and many of these sources can be avoided or reduced by radar design, radar operation and signal processing algorithms. Thus, design and construction cost of the radar is a major factor.

However, a cost-effective system that satisfies tracking requirements can be designed with the knowledge of how much error can be tolerated in the system. The errors that are affecting the system performance can be listed as follows:

- Radar dependent errors
- Target dependent errors
- Propagation errors

Radar dependent errors can be receiver thermal noise or servo-system noise. Multipath and irregularities in different atmospheric layers can constitute examples to the propagation errors.

Target dependent errors are amplitude fluctuation in return signal, angle glint and range glint. Target noise is applicable to all complex targets that are large with respect to wavelength of illumination [2]. At this point, the extended target concept becomes important.

The most common radar targets cannot be considered as a point-like target in current radar applications. Thus, their spatial extents in each coordinate must be taken into account. Such complex targets which consist of spatially separated scattering elements can cause significant measurement errors.

The errors may be large enough and deterministic about the overall accuracy of the radar. If this error (glint error) is not small compared to the other error components, the target is considered as extended [5]. It should also be noted that the same target may be supposed as a point-like at long ranges but extended at short ranges.

The glint errors and the glint reduction techniques are presented and discussed in the next chapters in detail.

1.2. Motivation

Glint error can be the dominant error source for short range targets. Homing guided missiles, for example, suffer glint error. For such systems, the accuracy of the target bearing angle is very critical. Since glint error is a target dependent error source, the reduction techniques are important as much as the design of the radar system.

Although tracking filters are efficiently used in radar systems, non-Gaussian noise like glint can make the tracking filters inefficient. Therefore, reduction techniques for glint error must be employed for more accurate angle and position of the target. The need for the performance evaluation of the reduction techniques is the motivation for this thesis.

Consequently, this thesis deals with the use of the glint reduction techniques. These techniques are evaluated in a comparative manner and the improvements that can be gained are presented.

1.3. Thesis Objectives

This thesis aims to examine the performance of the glint reduction techniques. The enhancement of improvements on reduction performance is also focused in the thesis. To that end, a multi-point scatterer target is used as target model for gathering target return signal. Simulation needs to be adoptable for acquiring suitable data for different reduction techniques.

Therefore, this thesis aims to accomplish the objectives listed as follows:

- Research of glint reduction techniques
- Simulation of target echo signal with glint
- Performance evaluation of glint reduction techniques
- Investigation of the effects of target and system parameters on reduction
- Comparison of reduction techniques

The next section in this chapter gives the thesis outline.

1.4. Outline of the Thesis

After providing an introduction to motivation and objects of this thesis, a basic illustration of glint will be given for two-point target in Chapter 2. Chapter 3 will present the literature studying glint. The direction finding methods and the simulation models are the other issues covered in Chapter 3. Chapter 4 investigates the basic principles on glint error, the glint reduction techniques and the possible reduction algorithms along with the use of these techniques. Chapter 5 examines the reduction methods, the effect of target and system parameters. Chapter 5 also discusses the reduction results of the techniques in a comparative manner. Finally, conclusions are presented in Chapter 6 and possible future work is discussed for prospective enhancements.

CHAPTER 2

TWO POINT TARGET GLINT ILLUSTRATION

2.1. Two Point Target

Glint is originated from complex targets which are composed of many point scattering elements. The phase fronts generated by each scatterer may cause the phase front seen by radar to point outside the extent of target. To illustrate this phenomenon a two point target is used. Even with this simple target configuration, the glint may show itself. The target geometry is given in Figure 2.1.

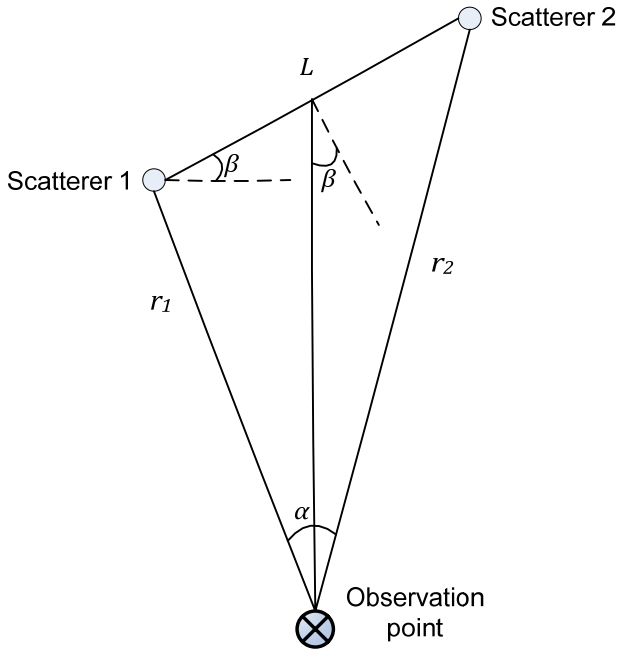

Figure 2.1 – Target geometry for dumbbell model

Two points are separated by distance L. The points are on the same plane with the observation point at range r_1 and r_2. The dimension in range which can be called as target depth is $D = L\sin(\beta)$ and the dimension in crossrange which can be called as target width is $W = L\cos(\beta)$ since the target orientation angle is β.

2.2. Basic Glint Relations of Two Point Target

In this section, the physical origin of glint will be presented following [5]. Glint error will be examined on simple two point target model which has the geometry in Figure 2.1.

The reflected field of a point target has a spherical phase front. Tracking radar antennas aim to measure the normal to the phase front. For a point target, this will not produce error in angular measurements.

Since the target has two point source components in our case, two different spherical phase fronts will reach the observation point or the radar. These two phase fronts may interfere with each other and the center of target may not be pointed by the normal of the resultant phase front. In this case, it is called apparent center that is pointed by the phase front's normal.

The position of the apparent center is dependent on the relative phase and amplitudes of point source echoes. This dependence states that the change in phase and amplitude, for example due to the target rotation, will cause the apparent center to wander. Therefore, fluctuations in the measured target angle may appear as well as fluctuations in resultant echo amplitude. The range accuracy will also be affected by the interference of phase fronts. To sum up, the wandering in the apparent center will generate glint noise components in angle, range and velocity estimations for an extended target.

Because of the physical origin of these noise components, radar systems must consider glint noise as a basic characteristic of targets. Therefore, it is important to analyze the characteristics of these noise components and their relationships.

The analysis of the two point target assumes that the separation L is small compared to target range. The total signal received at the observation is the sum of

two individual signals echoed by the point sources. The signal can be expressed as follows:

$$S_t(t) = S_1(t) + S_2(t) \tag{2.1}$$

where $S_1(t)$ and $S_2(t)$ are the field intensities of individual specular points. These can be written as:

$$S_1(t) = E_1 e^{j(w(t-t_1)+\emptyset_1)} \tag{2.2}$$

$$S_2(t) = E_2 e^{j(w(t-t_2)+\emptyset_2)} \tag{2.3}$$

where t_1 and t_2 are the two way trip time of the radiated electromagnetic energy. $\emptyset_1$ and $\emptyset_2$ are the initial phases of the reflecting elements due to the reflection differences between them. Total received signal also can be expressed in a similar manner as:

$$S_t(t) = E_t e^{j(wt-\emptyset_t)} \tag{2.4}$$

Let the phase offset of S_1 be $\varphi_1 = w(t-t_1) + \emptyset_1$ and the phase offset of S_2 be $\varphi_2 = w(t-t_2) + \emptyset_2$. Then,

$$\begin{aligned} {E_t}^2 = {E_1}^2\cos^2(\varphi_1) + {E_2}^2\cos^2(\varphi_2) + 2E_1E_2\cos(\varphi_1)\cos(\varphi_2) \\ + {E_1}^2\sin^2(\varphi_1) + {E_2}^2\sin^2(\varphi_2) + 2E_1E_2\sin(\varphi_1)\sin(\varphi_2) \end{aligned} \tag{2.5}$$

$$E_t = \sqrt{{E_1}^2 + {E_2}^2 + 2E_1E_2\cos(\varphi_1 - \varphi_2)} \tag{2.6}$$

After finding the amplitude of the resultant signal, the phase offset, $\emptyset_t$, can be derived from the equation

$$E_t e^{-j\emptyset_t} = E_1 e^{-j(wt_1-\emptyset_1)} + E_2 e^{-j(wt_2-\emptyset_2)} \tag{2.7}$$

This equation can be reformulated as

$$E_t e^{j\emptyset_t} = e^{j\left(\frac{w(t_1+t_2)}{2}\right)}\left(E_1 e^{j\left(\frac{w(t_1-t_2)}{2}\right)}e^{-j\emptyset_1} + E_2 e^{j\left(\frac{w(t_2-t_1)}{2}\right)}e^{-j\emptyset_2}\right) \tag{2.8}$$

The $\left(\frac{w(t_2-t_1)}{2}\right)$ term is the half phase difference due to the delay times and can be extracted from the geometry as:

$$\theta = \left(\frac{w(t_2 - t_1)}{2}\right) = \frac{w}{2}\left(\frac{2Lsin(\beta)}{c}\right) = \frac{2\pi}{\lambda}Lsin(\beta) \tag{2.9}$$

By using this, Equation 2.8 becomes

$$E_t e^{j\emptyset_t} = e^{j\left(\frac{w(t_1+t_2)}{2}\right)}\left(E_1 e^{-j(\theta+\emptyset_1)} + E_2 e^{-j(\theta-\emptyset_2)}\right) \tag{2.10}$$

Thus, the phase of the resultant signal can be expressed as:

$$\emptyset_t = \frac{w(t_1 + t_2)}{2} - \tan^{-1}\left(\frac{E_1 \sin\left(\emptyset_1 + \frac{2\pi}{\lambda}Lsin(\beta)\right) + E_2 \sin\left(\emptyset_2 - \frac{2\pi}{\lambda}Lsin(\beta)\right)}{E_1 \cos\left(\emptyset_1 + \frac{2\pi}{\lambda}Lsin(\beta)\right) + E_2 \cos\left(\emptyset_2 - \frac{2\pi}{\lambda}Lsin(\beta)\right)}\right) \tag{2.11}$$

The resultant phase is important to derive the glint error equations for the two point target. The derivations related with glint error are based on Figure 2.2. The figure shows the apparent center of the target and the angle with range shifts from the real center of target.

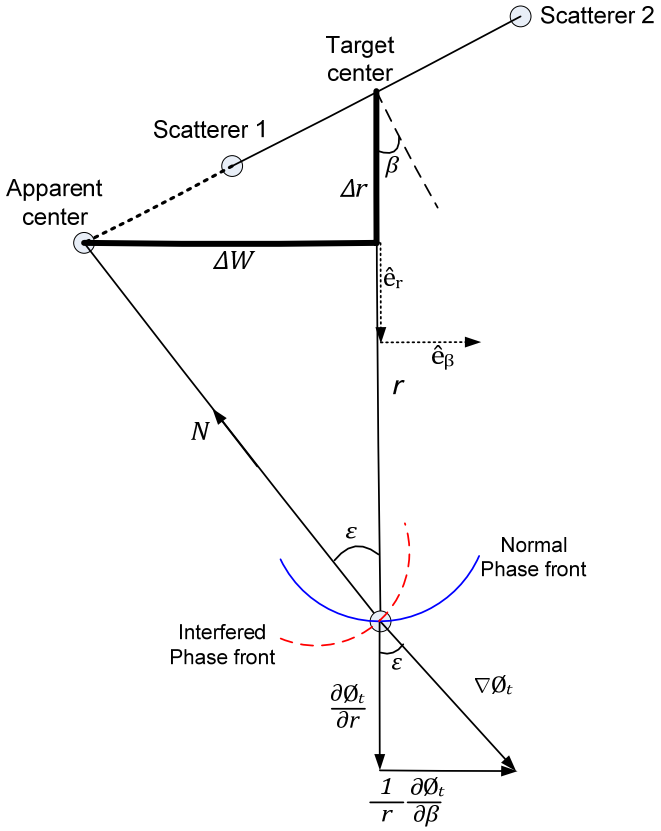

Figure 2.2 – Apparent center shift of two point target

The apparent center is shifted by ΔW in crossrange and Δr in range direction. The normal of resultant phase front is pointing to the apparent center. To determine the apparent center, gradient of resultant phase should be found. For this reason the phase is expressed as a function of the polar coordinates r and β:

$$\emptyset_t = \frac{2w}{c} r + \emptyset(\beta) = \frac{4\pi}{\lambda} r + \emptyset(\beta) \tag{2.12}$$

where $r = (r_1 + r_2)/2$ and $\emptyset(\beta)$ is the tangent inverse term in Equation 2.11.

The gradient of the phase front is in the same direction with the normal to the phase front. The direction of apparent center seen by the observation point is the opposite vector of the gradient of the phase vector. The wandering center of the target to the apparent center generates an angular error of ε. The gradient of the phase front is

$$\nabla \emptyset_t(r, \beta) = \frac{\partial \emptyset_t}{\partial r} \hat{\mathrm{e}}_{\mathrm{r}} + \frac{1}{r} \frac{\partial \emptyset_t}{\partial \beta} \hat{\mathrm{e}}_{\beta} \tag{2.13}$$

where $\hat{\mathrm{e}}_{\mathrm{r}}$ and $\hat{\mathrm{e}}_{\beta}$ are the unit vectors for the respective polar coordinates r and β.

From the geometry given in Figure 2.2, the angular error can be found as:

$$\varepsilon = \tan^{-1}\left(\frac{\frac{1}{r}\frac{\partial \emptyset_t}{\partial \beta}}{\frac{\partial \emptyset_t}{\partial r}} \right) = \tan^{-1}\left(\frac{\lambda}{4\pi r} \frac{\partial \emptyset_t}{\partial \beta} \right) \tag{2.14}$$

The linear error ΔW can also be given by the following:

$$\Delta W = r * \tan(\varepsilon) = \frac{\lambda}{4\pi} \frac{\partial \emptyset_t}{\partial \beta} \tag{2.15}$$

By differentiating Equation 2.11 with respect to β, $\frac{\partial \emptyset_t}{\partial \beta}$ can be found as:

$$\frac{\partial \emptyset_t}{\partial \beta} = \frac{2\pi}{\lambda} L cos(\beta) \frac{{E_2}^2 - {E_1}^2}{{E_1}^2 + {E_2}^2 + 2E_1E_2 \cos(\varphi_1 - \varphi_2)} \tag{2.16}$$

Therefore the angular and linear errors are derived as followings:

$$\tan(\varepsilon) = \frac{L cos(\beta)}{2r} \frac{{E_2}^2 - {E_1}^2}{{E_1}^2 + {E_2}^2 + 2E_1E_2 \cos(\varphi_1 - \varphi_2)} \tag{2.17}$$

$$\Delta W = \frac{Lcos(\beta)}{2} \frac{{E_2}^2 - {E_1}^2}{{E_1}^2 + {E_2}^2 + 2E_1E_2\cos(\varphi_1 - \varphi_2)} \tag{2.18}$$

The error in the range Δr can also be expressed as

$$\Delta r = \frac{Lsin(\beta)}{2} \frac{{E_2}^2 - {E_1}^2}{{E_1}^2 + {E_2}^2 + 2E_1E_2\cos(\varphi_1 - \varphi_2)} \tag{2.19}$$

First terms in the above equations are related with the half angle and half width extensions of the target. Therefore, normalized angular error factor can be presented as:

$$\varepsilon_{norm} = \frac{\tan(\varepsilon)}{\tan\left(\frac{\alpha}{2}\right)} = \frac{\Delta W}{W/2} = \frac{\Delta r}{D/2} = \frac{{E_2}^2 - {E_1}^2}{{E_1}^2 + {E_2}^2 + 2E_1E_2\cos(\varphi_1 - \varphi_2)} \tag{2.20}$$

First result of the normalized error equation is that error depends on the individual amplitudes of the echo signals and the phase difference between them. Another fact is that ε_{norm} can take any value between $-\infty$ and ∞. Thus, the apparent center may wander far beyond the physical extent of the target. For better understanding of the normalized factor, the interpretation of the factor can be given by the followings [5,6]:

- If $E_1 = 0$, error factor is 1 and the angular glint which is produced by only scattering element 2 is $\alpha/2$. Thus the radar tracks the scatterer 2.
- If $E_2 = 0$, error factor is -1 and the angular glint which is produced by only scattering element 1 is $-\alpha/2$. Thus the radar tracks the scatterer 1.
- If $E_1 = E_2$ and $\varphi_1 - \varphi_2 = \mp\frac{\pi}{2}$, error factor is 0 and the angular glint is also 0. Thus the radar tracks the geometrical center of the target.
- If $E_1 = E_2$ and $\varphi_1 - \varphi_2 = \mp\pi$, error factor is $\mp\infty$ and the angular glint is also infinite. Thus the radar cannot track the target at all.

The normalized error factor can be reformulated as in Equation 2.21 [5]. By using this new expression, sample values of the normalized error factor are shown in Figure 2.3.

$$\varepsilon_{norm} = \frac{1 - z^2}{1 + z^2 + 2z\cos(\varphi)} \quad , \; where \;\; z = E_1/E_2 \tag{2.21}$$

The absolute value of the error factor is presented for simplicity. The values which are greater than one indicate that the apparent center is outside the target. Thus, tracking the target may be impossible if the magnitude of error factor is much greater than one.

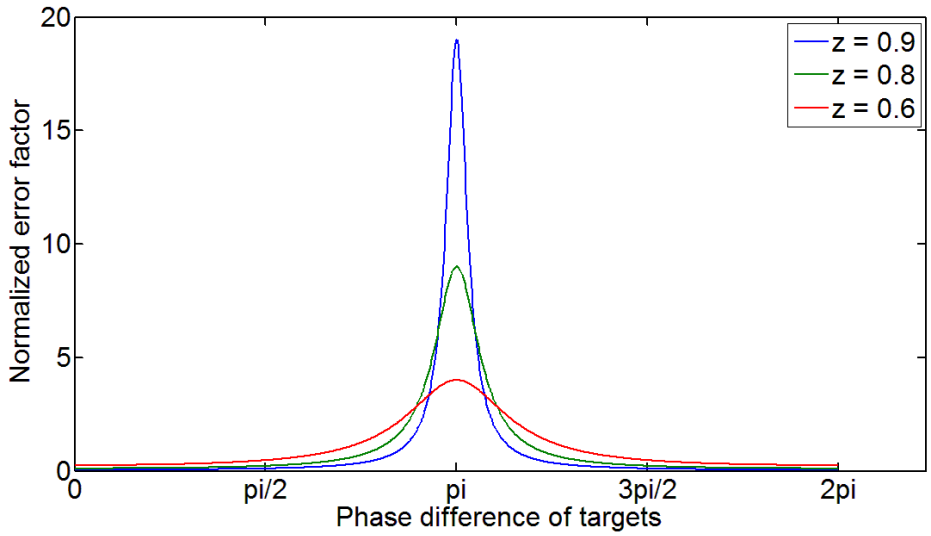

Figure 2.3 – Normalized error factor for two point target

As it is seen from Figure 2.3, the glint error becomes very large especially for phase differences close to π. If the echo amplitudes of the scattering elements are closer, the error tends to cause critical measurement failures in tracking the apparent center of the target.

Although this model cannot represent the typical radar targets, it can simply illustrate how glint phenomenon is generated by the targets. It also gives information about the statistical properties of glint. This basic model also can be used to investigate glint reduction techniques.

It is useful to consider the following reformulated normalized error factor expression:

$$\varepsilon_{norm} = \frac{1 - z^2}{|1 + ze^{j\varphi}|^2} \tag{2.22}$$

The denominator of the Equation 2.22 can be regarded as the amplitude of the total received signal. If $\left|1 + ze^{j\varphi}\right|^2$ term in the equation tends to zero and the amplitude ratio of scatterers is close to one, the glint error becomes noticeable to be taken into account. This property states that the amplitude of the received signal and the glint error are negatively correlated quantities. This feature will be reissued in the following chapters.

The negative correlation property also provides a basic intuition on how to mitigate the glint error due to scattering characteristics of the target. The phase of the target signal can be sampled at multiple points which may generate independent samples. The sampled points can be used with the purpose of generating reduction algorithms. This feature is the basis of the diversity techniques and the diversity selection methods.

CHAPTER 3

GLINT BACKGROUND AND SIMULATION MODEL

3.1. Direction Finding

Modern tracking radars need to utilize systems that generate information about the target's angle and range position in both azimuth and elevation. In this section of this chapter, angle tracking, i.e. direction finding, techniques will be presented. One of the presented techniques will be used in the simulations for measuring the glint as the deviation from the target geometric center. In this context, the historical and theoretical development of the angle tracking is important, since glint is a problem which is related with the measuring of the target position.

Sequential lobing, conical scan and monopulse techniques are mentioned here as direction finding methods.

Sequential lobing or lobe switching can be said to be one of the first tracking techniques used in the early radar systems. Although its implementation is simple and straightforward, tracking performance is limited with pencil beam width and switching mechanisms, i.e. electronic and mechanic switching [3].

Two or more switched beams are received and compared by radar in sequential switching. The voltage level difference between two signals is the basic concept in this method. If the target is on the tracking axis, difference signal will be zero. If the target is not on the tracking axis, the difference will be a nonzero value. The difference and its sign are used to move the antenna to the necessary direction. By doing this, it is aimed to make the difference signal zero [3].

Conical scanning, on the other hand, is a logical extension of sequential lobing [2,3]. The beam in this method which is a pencil beam is continuously rotated about the tracking axis [7]. This rotation which is achieved by either antenna movement or a rotating feed forms a narrow cone [3,7]. This method has been used intensively during and after World War II [7].

In conical scanning method, the signal received from the target is an AM modulated like signal dependent on the beam scan frequency and the squint angle between the target and the antenna's line of sight [3]. The angle information is extracted from this modulated signal to drive the servo system. When the tracking axis coincides with the target, then the modulation on the received signal is zero. Thus, no antenna movement will be required in this case [3].

Monopulse techniques are being used in most radar systems instead of conical scanning. The conical scanning performance is sensitive to the amplitude scintillations induced by the target. There is also a limitation in the electronic and mechanical scan rate because of the need of minimum 2 returns per coordinate [3]. For this reason, simultaneous lobing, i.e. the monopulse techniques, are analyzed in the next sections.

3.1.1. Monopulse Techniques

The amplitude scintillations and the weakness against amplitude jamming properties of conical scanning and sequential lobing techniques have created the need for the monopulse techniques. This technique is developed for lobing required spatial volumes simultaneously for extracting the angle of arrival [2].

Multiple beams are used in a single pulse for generating the sum and difference echoes reflected from the volume. The amplitude based monopulse and the phase based monopulse techniques are presented in the next sections. Phase comparison monopulse technique is used for the simulations of glint reduction algorithms. Nevertheless, both are evaluated to see which one is more prone to glint error.

3.1.1.1. Amplitude Comparison Monopulse

Amplitude comparison monopulse is based on the signals which have same phase and different amplitudes [3]. The beams used can be illustrated as in Figure 3.1 in one plane. The beams intersect along the tracking axis.

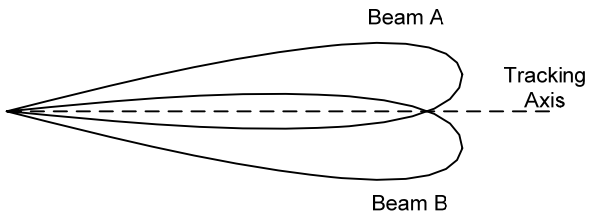

Figure 3.1 - Amplitude monopulse antenna pattern

Amplitude comparison monopulse technique generates sum and difference of the target echoes and this information is used to estimate the target angle. An example of beam patterns with sum and difference patterns is given in Figure 3.2. The difference pattern to the sum pattern ratio is also given in Figure 3.2. The example is following typically used sinc pattern for each channel.

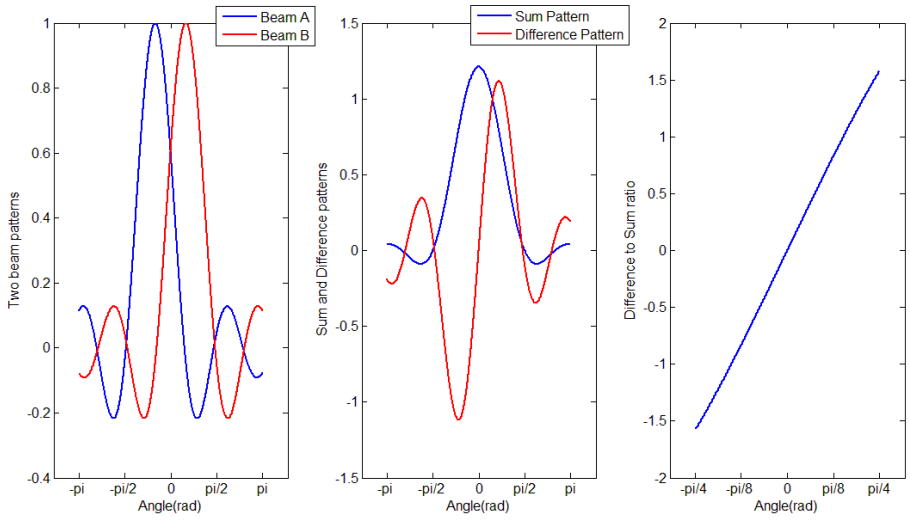

Figure 3.2 - The beam patterns, sum and difference patterns and the difference to sum ratio

The difference to sum ratio is used for angle of arrival calculation. Let E_A and E_B be the echoes returned for beams A and B. Then the target angle and the sign of the angle can be found with the following equations.

$$\text{argmin}_\theta = \left(\left|\frac{\Delta(\theta)}{\Sigma(\theta)}\right| - \left|\frac{E_A}{E_B}\right|\right) \tag{3.1}$$

$$\theta = \theta * \text{sign}\left(\frac{E_A}{E_B}\right) \tag{3.2}$$

In practice, the sum and difference patterns are generated for discrete angle values, thus the precision of the calculated angle is limited with the resolution of the generated antenna patterns.

3.1.1.2. Phase Comparison Monopulse

While the amplitude is important for amplitude comparison monopulse, phase comparison monopulse is based on the signals which have same amplitudes, but different phases. For this reason, multiple antennas with overlapping illumination are used to extract the desired information [2].

A simple phase comparison radar can be illustrated as in Figure 3.3. The geometry is given for only one plane. As it can be seen from the geometry, a phase difference between the echoes at different antennas will be generated in this system.

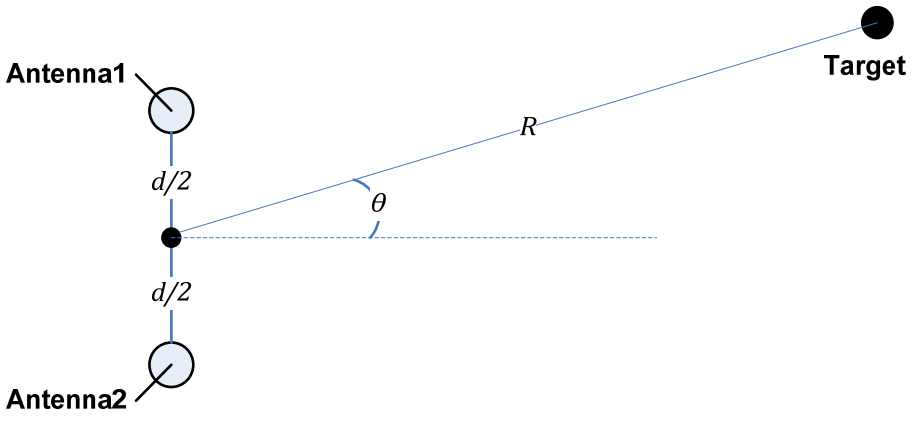

Figure 3.3 - Phase comparison monopulse geometry

By assuming $d \ll R$ and dropping the echo amplitude, the echoes at the antennas can be expressed from the geometry as:

$$E_1 = e^{j2\pi f\frac{2R}{c}}e^{-j2\pi f\frac{d\sin(\theta)}{c}} \quad , \quad E_2 = e^{j2\pi f\frac{2R}{c}}e^{j2\pi f\frac{d\sin(\theta)}{c}} \tag{3.3}$$

Although the angle can be easily calculated from the phase difference between the signals, this method is prone to performance degradation. Thus, using sum and difference of the channels can generate more stable angle estimation results [3]. The sum, difference channels and the difference to sum channel ratio result in the followings:

$$\Sigma(\theta) = E_1 + E_2 = e^{j2\pi f\frac{2R}{c}} * 2 * \cos(kd\sin(\theta)) \tag{3.4}$$

$$\Delta(\theta) = E_2 - E_1 = e^{j2\pi f\frac{2R}{c}} * 2\mathrm{j} * \sin(kd\sin(\theta)) \tag{3.5}$$

$$\frac{\Delta(\theta)}{\Sigma(\theta)} = j\tan(kd\sin(\theta)) \tag{3.6}$$

where k, wave number, is $2\pi f/c$. It is seen that, the difference to sum ratio is purely imaginary. As a result, the target angle can be calculated from below equation.

$$\theta = \sin^{-1}\left(\frac{\tan^{-1}\left(\mathrm{imag}\left(\frac{\Delta(\theta)}{\Sigma(\theta)}\right)\right)}{kd}\right) \tag{3.7}$$

This result is used in the simulations in the calculation of target angle as a reference to the glint error calculation.

3.2. Prior Glint Investigation

In this section of this chapter, the literature research on glint phenomenon is presented in chronological order. Glint has been studied over many years starting from late 1940's up to the present time. Glint is majorly emphasized by the military applications which demand more accurate information on target position. As a result, much of the work is either classified or limitedly distributed. Therefore, the investigation presented here is comprised of the accessible work in the literature.

In the early radars, target scintillation effects were simply treated as the reason of target fading. This scintillation in the echo amplitude also affects the maximum range that can be detected by the search radar [10].

The effects of target scintillation in the target tracking radar were observed in the prewar experimental tracking radars and throughout the World War II. As mentioned in the previous section, early tracking radars use conical scan or lobing mechanism to estimate the target angle. The performance affected by the target scintillation was considered the result of the amplitude modulation produced by scanning or lobing. This thought also agrees with the effects of propeller modulation on tracking noise [8-10].

U.S. Naval Research Laboratory has started a study on noise in tracking radars in 1947 with Hughes Aircraft Company, MIT and several governmental and private organizations [8-10]. The outcomes of this research were revealed by mid-fifties.

There were two approaches on glint modeling, namely statistical and deterministic approaches. Delano published the first unclassified paper [11] which uses statistical techniques to model glint phenomenon. This paper has served as the basis for other glint researches. Delano derived the probability density function of a tracker output fluctuation.

Single tracking channel and a linear array of isotropic scatterers which have independent amplitude and phase characteristic are used by Delano and the resultant density was Student-t distribution with two degrees of freedom. Delano used constant amplitudes and independent random phases, since it is enough for Rayleigh statistics. A significant result from his analysis was that the apparent target location goes beyond the target's physical extent 13.4 percent of the time.

By using Delano's results and several different types of target motion, Muchmore studied the amplitude and glint spectra [24]. Although, both Delano's and Muchmore's results were criticized by Peters and Weimer [25], the spectra showed similar results with the experimental result as reported by [9] and [10].

Gubonin also studied glint with a different interpretation and derived statistics related to glint [26]. He reached the same results with Delano, but the derivations of Gubonin present more general results.

Dunn and Howard presented the scintillation noise researches in radar tracking [8] which are carried through analysis, measurement and simulation techniques at Naval Research Laboratory. The results of some classified studies are summarized in their paper in a historical manner. One of the main findings was that the angle error is by far the largest error component in tracking noise at short ranges.

It is also mentioned that AGC may affect the target noise to the tracking system under certain conditions. They noted that slow-acting AGC is especially important for medium and/or long ranges. For this reason, they recommend a wide bandwidth fast-acting AGC. The effect of AGC is not studied in the context of this thesis.

Glint error is accepted to be originated from the phase front distortion concept. However, Dunn and Howard showed the energy-flow tilt concept can be used equivalently with phase front distortion [17]. They present the method of glint computation by using the Poynting vector components.

There are generally efforts for statistical glint modeling methods in the literature. Borden and Mumford developed a formulation for glint and RCS models with individual and cross statistics [27].

Unification of two angular glint concepts, namely phase front distortion and energy flow tilt concepts, are discussed and compared by Yin and Huang [29]. They suggest using the phase gradient method to obtain angular glint in practice.

Borden has covered the glint problem in his report [14]. He discussed some issues such as “What is glint” and “How can it be solved?”. His paper may be a good starting point for understanding glint error and glint reduction approaches.

Angular glint modeling and simulation studies are continued with developing computation environments. RCS and angular glint simulations for complex targets are discussed in these papers [30, 31].

The reduction of glint techniques is studied in the literature by various researchers. A practicable reduction research which is based on RCS weights are presented by Zhen-yu [32]. Synthesis of the simulation and real data experiments are discussed to show the effectiveness of the reduction technique.

The presented investigation of glint is only a summary of glint literature. Several conclusions can be drawn from the glint studies. However, various researchers argued glint phenomenon from different perspectives. The lack of unity of purpose in glint investigations may misguide uninitiated readers.

The modeling, as well as conducting experiments on glint is a hard task for radar engineers. Hardware in the loop simulations were studied for both simple and detailed examination of glint [28].

3.3. Glint Simulation Model

Glint phenomenon is basically a result of complex radar target scattering and the interfered phase front of the echoed illumination. This phenomenon is modeled in different ways as mentioned in previous section. The simulation model supports the illustration of the basic properties of glint error. In addition, the aim of reduction algorithms' evaluation is taken into account in the simulation model as a major factor.

The statistical models are purely analytic models which are lacking of models of the target centroid motion due to different parameters. Statistical models may also demand stationary statistics and isotropic scatterers, which is not true in many cases.

Although, deterministic approach does not require any statistical stationarity and can keep the non-isotropic structure of scatterers, still all related information about individual scaterers are required for modeling. Nevertheless, the deterministic approach is chosen, since it reflects the nature of glint better than statistical techniques.

The model used for accomplishing the thesis objects consists of multiple scatterers on single target. The properties and the reduction algorithms' performance are presented for one target case. The target and radar are assumed to be in the same plane and the simulations are implemented only for x-y plane. The simulations can of course be extended for further analysis of multiple targets and tracking of them.

It is assumed in the model that all scatterers used in the simulation contribute to the echo signal for the same resolution cell. It is also assumed that the signal power of

the target is enough for detection and the target is detected. Thus, noise components other than glint error (target noise) are not considered in the simulation.

Coherent or non-coherent pulse integration methods are not used in the simulation since there is no detection in the simulation loop. Therefore, only the target signal in one resolution cell is considered rather than generating pulse-range matrix for the illuminated volume.

Monopulse direction finding is used as the reference in the calculation of angular glint error. The amplitude monopulse and the phase monopulse techniques are implemented. The correlative vector direction finding (CVDF) is also implemented for further comparison of the direction finding methods.

The scattering geometry, target return signal calculations and the target angle calculation are given in the next sections in this chapter.

3.3.1. N-Point Scattering Element Geometry

The target used in the simulations is comprised of multiple scatterers that make the target extended. These scatterers are placed randomly in a rectangular shaped region that models the target. The positions of the scatterers are uniformly distributed in the target dimensions. The geometry and the scatterers are shown in Figure 3.4.

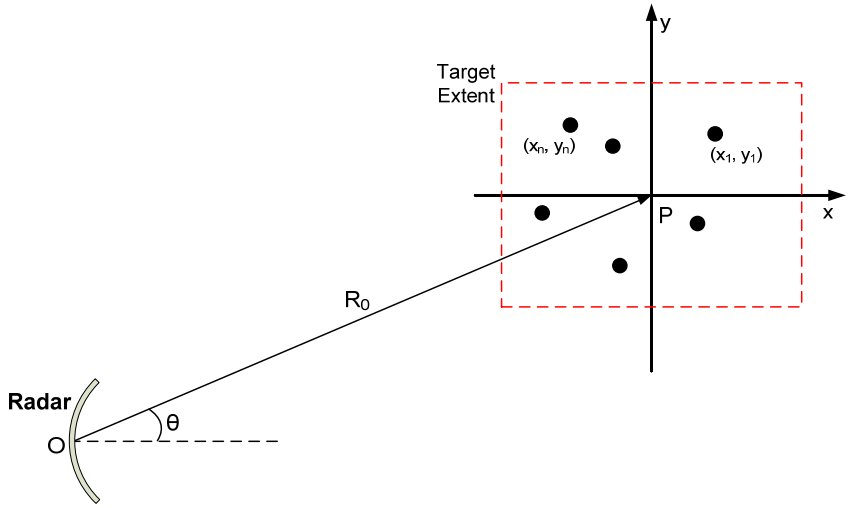

Figure 3.4 - General target and radar geometry for simulation

The target is placed in x-y plane at a range of R_0 and at an angle of θ. This point, P, is the geometric center of the complex target and the mean of the scatterers' position is zero with respect to this point.

Although glint phenomenon is considered as a randomly generated target characteristic, it is actually a deterministic function of many parameters like aspect angle, radar center frequency, scattering element characteristics etc. The effects of the glint can be observed on a stationary target and the effects are repeatable. Therefore, the relative target motion is generally ignored and the basic glint generation mechanisms are involved in the simulations. The target motion is only considered for ISAR like aspect diversity reduction which will be presented in next chapters.

3.3.2. Generating Target Return Signal

This section describes the target echo signal for each of the scatterers and the integration of them. Each scatterer has a complex scattering characteristic which is related with the physical properties of the target and the operational properties of the radar.

Two different return signals are generated with the purpose of target angle estimation. The phase monopulse technique requires two antennas which is not the case in Figure 3.4. The amplitude monopulse and CVDF techniques require two transmit/receive patterns.

The total received echo from n scatterers at radar can simply be expressed as:

$$E_t = \sum_{i=1}^{i=n} a_i e^{j\phi_i} * A_i e^{j\frac{2R_i}{c}} \tag{3.8}$$

$a_i = Random\ amplitude\ due\ to\ scatterer\ characteristic$

$\phi_i = Random\ phase\ due\ to\ scatterer\ characteristic$

$A_i = Amplitude\ due\ to\ illumination\ pattern$

$\frac{2R_i}{c} = Phase\ due\ to\ scatterer\ distance\ to\ the\ radar$

The random scattering parameters a_i and ϕ_i are chosen randomly for general glint error illustrations and general reduction schemes. However, these parameters depend on system parameters like frequency and polarization while depending also on the target angle and the aspect angle of the target. Although, these dependencies are investigated in the literature, reasonable modeling of single element scattering characteristic cannot be found.

The next chapters investigate the effects of diversity methods on glint reduction. For this reason, scattering parameters are needed for various frequencies and aspects. Taking these parameters as independent random variables for all frequencies and/or aspects will render the diversity analysis useless. At this point, the random amplitude of scattering is not as important as phase in glint analysis. Delano also mentions that same amplitudes are enough [11]. For this reason, the random amplitude is dropped from the return signal in diversity analysis. Although, the random phase of scatterers are important, this parameter is also dropped, since model of this phase component cannot be found in the available literature. Actually the random phase is added to the model but the dependency on frequency or aspect angle is dropped.

These scattering parameters will not be used as random for each center frequency or aspect angle in the analyses of the diversity methods. Nonetheless, illustrations and other analysis of glint error are still using totally random complex scattering characteristics.

3.3.2.1. Return Signal With Different Antennas

Spatially different antennas will have a phase difference for the target and this constitutes the basics of phase monopulse direction finding method. The antennas will have same patterns such that the amplitudes for each antenna and for each scatterer will be the same.

The echo signal at the antennas can be expressed as:

$$E_1 = \sum_{i=1}^{i=n} e^{j\phi_{i1}(f,\theta)} * e^{j\frac{2R_{i1}}{c}} \quad , \qquad where\ R_{i1} = \sqrt{{x_i}^2 + \left(y_i - \frac{d}{2}\right)^2} \tag{3.9}$$

$$E_2 = \sum_{i=1}^{i=n} e^{j\phi_{i2}(f,\theta)} * e^{j\frac{2R_{i2}}{c}} \quad , \qquad where\ R_{i2} = \sqrt{{x_i}^2 + \left(y_i + \frac{d}{2}\right)^2} \tag{3.10}$$

The scatterer random phases are taken the same for the different antennas, i.e. $\phi_{i1}(f,\theta)$ is equal to $\phi_{i2}(f,\theta)$. The dependence on frequency and aspect is dropped or taken as independent for different analysis types.

The sum and difference signals can easily be expressed as:

$$\Sigma_t = E_1 + E_2 \tag{3.11}$$

$$\Delta_t = E_2 - E_1 \tag{3.12}$$

3.3.2.2. Return Signal With Different Transmit/Receive Patterns

Amplitude monopulse and correlative vector direction finding methods requires two different patterns on either transmit or receive. The received amplitude in this case will be different and the phases will be the same. The patterns are chosen as simple sinc patterns for simulation purposes. The sinc function used in this thesis is the normalized form which is $\mathrm{sinc}(x) = \sin(\pi x)/(\pi x)$.

The patterns are taken 30 degree shifted from the main axis as:

$$P_1(\theta) = \mathrm{sinc}(\theta + 30°) \tag{3.13}$$

$$P_2(\theta) = \mathrm{sinc}(\theta - 30°) \tag{3.14}$$

The sum and difference pattern vectors are calculated as:

$$\Sigma(\theta) = P_1(\theta) + P_2(\theta) \tag{3.15}$$

$$\Delta(\theta) = P_2(\theta) - P_1(\theta) \tag{3.16}$$

The ratio of the patterns that are used in direction finding is calculated as

$$\Gamma(\theta) = \frac{\Delta(\theta)}{\Sigma(\theta)} \tag{3.17}$$

This ratio is evaluated only for the interval of $-\pi/4$ and $\pi/4$ since the pattern ratio is almost linear for this interval. Increasing the interval will break the monotonous behavior of the ratio and cause erroneous angle estimation for those angle values.

For these antenna patterns, the echo signals can be given similarly to the previous case as:

$$E_1 = \sum_{i=1}^{i=n} e^{j\phi_i(f,\theta)} * \mathrm{sinc}(\theta + 30°) * e^{j\frac{2R_i}{c}}, \qquad where\ R_i = \sqrt{{x_i}^2 + {y_i}^2} \tag{3.18}$$

$$E_2 = \sum_{i=1}^{i=n} e^{j\phi_i(f,\theta)} * \mathrm{sinc}(\theta - 30°) * e^{j\frac{2R_i}{c}} \tag{3.19}$$

The random phases of scatterers are taken to be the same for both patterns and the dependence on frequency and aspect angle is used properly for different analysis. The sum and difference signals are evaluated with the same equations (3.11, 3.12) from the previous case.

3.3.3. Target Angle Estimation

Angular glint error is measured with the reference of the estimated angle of the target. Angular error results given in this thesis are in absolute form. Averaging on absolute error is used for representing the Monte Carlo simulation results.

The simulations generally use the phase monopulse direction finding method, but amplitude monopulse and correlative vector direction finding methods are also investigated for comparison purposes.

The angle estimation equations require the received signals at sum and difference channels which are calculated with the equations given in previous section. The antenna patterns are the inputs of the target angle estimation methods.

The phase monopulse angle estimation uses Equation 3.7. The distance, d, should be sufficiently small so that it will not cause the phase to fold. Although this method gives more precise results than the other methods used, it is highly dependent on phase differences. Nonetheless, it is used in this thesis for simulation purposes.

On the other hand, the amplitude monopulse uses the amplitude ratios of the sum and difference channels. In this method, the measured ratio is compared with the antenna pattern ratio and the closest one is chosen as the angle of arrival. In other words, the angle that makes the below equation minimum is the target angle.

$$\text{argmin}_\theta = \left(|\Gamma(\theta)| - \left|\frac{\Delta}{\Sigma}\right| \right) \tag{3.20}$$

This method is using the amplitude data for angle estimation; as a result the sign of the estimated angle may be either positive or negative. Thus, the sign, s_θ, is found by the following:

$$s_\theta = \text{sign}\left(\frac{\Delta}{\Sigma}\right) \tag{3.21}$$

The angle output of the amplitude monopulse method is:

$$\theta = |\theta| * s_\theta \tag{3.22}$$

The correlative vector direction finding (CVDF) aims to correlate the measurements with the antenna manifold vector. It uses both the phase and the amplitude of the received echo signal. This method searches the maximum correlated point of the resulting correlation vector [12]. The sum and difference patterns for CVDF method should be Euclidian sense normalized, i.e.

$$\Sigma(\theta) = \frac{\Sigma(\theta)}{\sqrt{\Sigma^2(\theta) + \Delta^2(\theta)}} \quad , \quad \Delta(\theta) = \frac{\Delta(\theta)}{\sqrt{\Sigma^2(\theta) + \Delta^2(\theta)}} \tag{3.23}$$

With the normalized antenna manifold vectors in hand, the target angle is calculated with the below equation.

$$\text{argmax}_\theta = \Sigma_t^* * \Sigma(\theta) + \Delta_t^* * \Delta(\theta) \tag{3.24}$$

The resolution of the amplitude monopulse and CVDF techniques are limited to the resolution of the generated (by theoretically or experimentally) antenna manifold vectors. Further resolutions can be achieved by curve fitting methods. In the simulations the resolution of the manifold vector used is 0.1mrad (0.0057°) which is small enough compared to the angle glint errors.

3.3.3.1. Comparison of DF Methods

Three methods introduced in previous section are compared from the view point of glint errors. This analysis aims choosing one of the methods that will be used in simulations. For this purpose the configuration given in Table 3.1 is used. The scattering characteristic of each scattering element is random in this analysis, since special treatment on scatterers is not required.

Table 3.1 - Simulation configuration of DF methods comparison analysis

Target depth	5m
Target width	5m
Target angle	10deg
Target range	1000m
Random scatterers on target	10
Center Frequency	10GHz
Number of experiments	100

The simulation results are given in Figure 3.5. The mean of errors for all methods are at the level of 0.08° for this simulation. CVDF and amplitude monopulse method results are very close to each other. The phase monopulse method can give worse results than the others. However, there are results that are better for phase monopulse method.

The processing of phase monopulse is easier than the other two methods. CVDF and amplitude monopulse methods are searching the minimum or maximum for the corresponding vector. Although using amplitude information of signal is less fragile to phase induced errors, the phase monopulse DF method is chosen because of its simple and fast angle calculation.

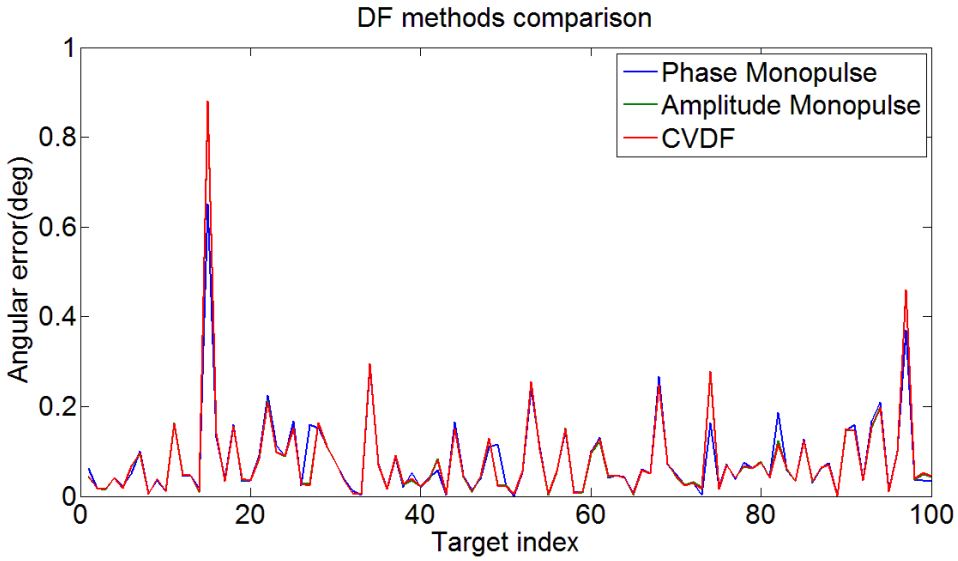

Figure 3.5 – Comparison of DF methods

CHAPTER 4

GLINT PROPERTIES AND REDUCTION METHODS

4.1. Introduction

This chapter aims to present the basic glint properties which explain the general nature of the glint phenomenon. These properties will demonstrate the glint error relationships with different parameters. The behavior of glint will also be supported with the glint simulations for better understanding of the phenomenon.

The investigation of properties will lead the main focus to the glint reduction techniques. The requirement of glint reduction is also a fundamental result of the glint properties.

After presenting the fundamental glint characteristics, the reduction methods that will be investigated in this thesis will be introduced. In addition, the main ideas of the reduction techniques will be presented.

Finally, the reduction mechanisms on reduction methods will be analyzed with the simulated target data. The effects of the reduction mechanisms will be shown in a comparative manner.

4.2. Glint Properties

Despite the random characteristics of target glint, the description and the understanding of the phenomenon is simple. Glint properties related to the radar tracking can be presented by investigating the simple complex scattering mechanisms.

A tracking radar system deals with the problem of finding normal to the phase front which is radiated back from the target. The examination of phase front for N-point

element target or a simple two-point element “dumbbell” target are used to investigate the properties of glint error.

Three basic properties that will be introduced in this section can be briefly given as the followings:

1) Targets that are closer to the radar are prone to angular glint error
2) Target echo amplitude is negatively correlated with the glint
3) Larger sized targets are prone to glint error

Next sections will present the related information with the above materials. The properties will also be investigated via simulations.

4.2.1. The relationship between glint and target range

Target range effect is discussed earlier implicitly while describing the extended target concept. The extended targets become point like targets when the target is far away from the radar. From this point of view, it can easily be concluded that targets closer to the radar are more likely to generate glint.

The phase front and phase gradient geometry is given in Figure 2.2. In Chapter 2, angular glint error is also formulated by the following:

$$\tan(\varepsilon) = \frac{\lambda}{4\pi r}\frac{\partial \phi_t}{\partial \beta} \tag{4.1}$$

This formula claims that the angular glint is directly proportional to the aspect angle derivative of the total received signal phase. The expression also shows that the angular glint error is inversely proportional to the target range. Although angular error is higher for closer ranges, linear glint error is not dependent on range, i.e,

$$r * \tan(\varepsilon) = \frac{\lambda}{4\pi}\frac{\partial \phi_t}{\partial \beta} \tag{4.2}$$

Although these findings describe the general behavior of glint error, a glint error spike may occur for some scattering scheme and can cause large errors that can violate the above equations. These equations should be treated as likelihoods for target range dependence.

The dependence of glint error on target range is simulated for the given configuration in Table 4.1. The scattering characteristic of each scattering element on target is chosen randomly, since this analysis does not require special treatment on scatterers.

Table 4.1 - Simulation configuration of range effect analysis

Target depth	5m
Target width	5m
Target angle	10deg
Simulated minimum target range	10m
Simulated maximum target range	1000m
Random scatterers on target	10
Center Frequency	10GHz
DF Method	Phase monopulse
Number of experiments for each range	1000

The results of the simulation are shown in Figure 4.1. The results are given with the expected results for comparison.

The simulation result shows that the target range is an increasing factor on angular glint error as expected. On the other hand, the linear error in target's position is not altering very much and can be treated as constant.

Figure 4.1 shows the average range effect on glint error; however the instantaneous effect may differ from this. A single run simulation result is given in Figure 4.2 to show spiky nature of glint error. Nevertheless, the range effect can be seen also from the single run simulation.

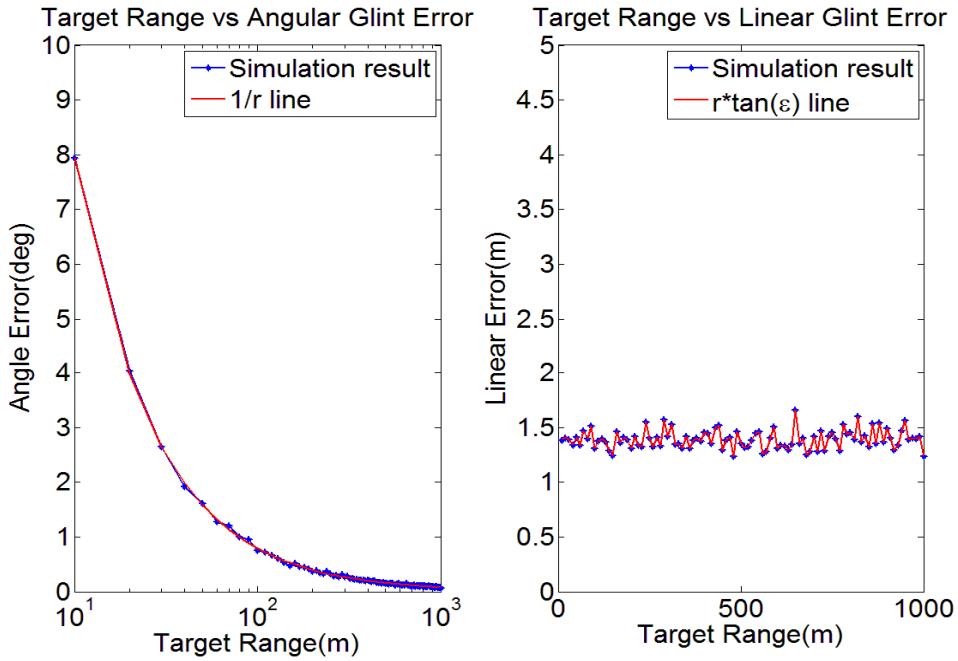

Figure 4.1 - Average target range effect simulation results

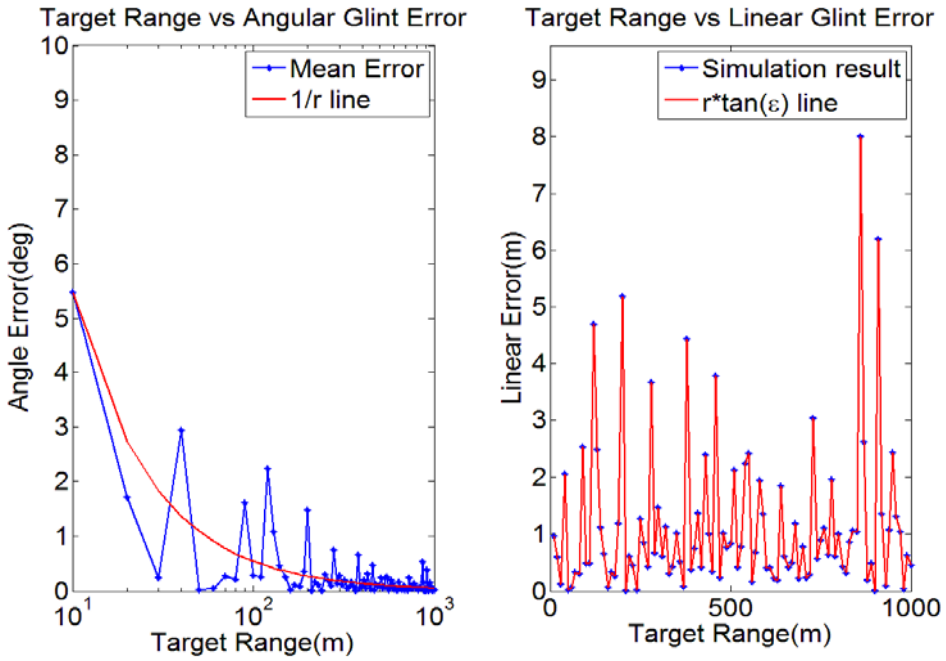

Figure 4.2 - Single run target range effect simulation results

4.2.2. The relationship between glint and echo amplitude

Throughout the researches on tracking problem, the amplitude fades are seen as one of the reasons of the tracking errors. For example, simultaneous lobing (monopulse) is studied against sequential lobing which generates a modulated signal at its output. However, it is understood that the amplitude fades can originate from target itself.

The two point target discussion in Chapter 2 also simply investigates the correlation between the echo amplitude and glint error. The normalized error equation 2.22 shows that the glint error tends to increase if the total echo from two scattering elements is decreasing.

On the other hand, Borden [14] has developed an expression for multiple scatterer case. He derived the relationship given below which presents the behavior of aspect angle derivative of echo signal phase around the glint spike. The expression assumes that the change in aspect angle is small.

$$\frac{\partial \phi_t}{\partial \beta} \propto \frac{1}{|E_t(k,\beta)|} \frac{\partial |E_t(k,\beta)|}{\partial \beta} \tag{4.3}$$

$E_t(k,\beta)$ is the total echo amplitude, and ϕ_t is the total echo phase. The dependence of amplitude to wave number, k, is also shown.

The dependence of glint error and the echo amplitude can be drawn by using Equations 4.1 and 4.3. If the echo amplitude goes to zero, the derivate term will increase and the $1/|E_t(k,\beta)|$ factor will cause the glint error to spike. This demonstrates the negative correlation between glint and echo amplitude [14].

The correlation between echo amplitude and glint error is observed also in simulations. Table 4.2 is used for this simulation. The target scatterer positions and the complex characteristic of each scatterer are random and independent in this simulation, since this analysis requires the general behavior of glint error.

Figure 4.3 and Figure 4.4 are given below for better understanding the amplitude-glint correlation. Angular glint errors are given in absolute form for easy interpretation of figures. Ten of the results which have the minimum amplitudes are marked in both figures.

Table 4.2 - Simulation configuration of amplitude-glint correlation analysis

Target depth	5m
Target width	5m
Target angle	10deg
Target range	1000m
Random scatterers on target	10
Center Frequency	10GHz
DF Method	Phase monopulse
Number of experiments	1000

Figure 4.3 shows that higher angular errors correspond to lower echo amplitude values. $1/|E_t(k,\beta)|$ line is given as a reference to the results and angular error seems to follow the relationship given in Equation 4.3. It can also be said that while the mean and the variance of angular error are not large, the error can take high values.

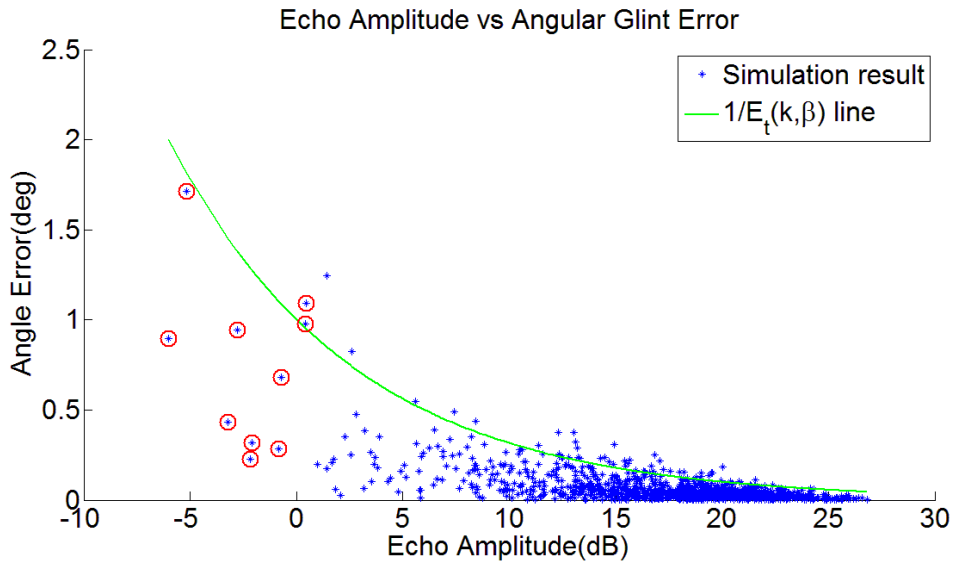

Figure 4.3 - Scatter-plot of echo amplitude and absolute angular error results

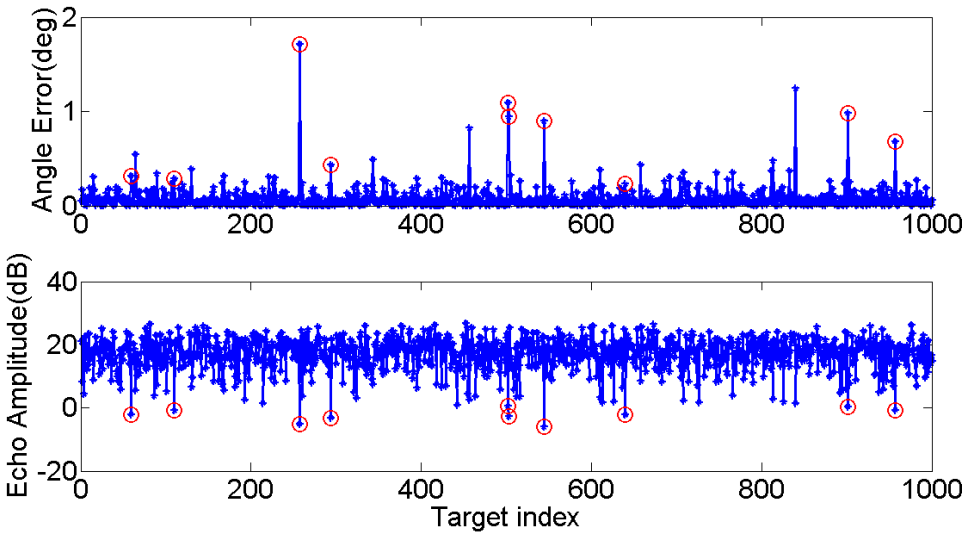

Figure 4.4 - Angular glint errors and corresponding echo amplitude values

Figure 4.4 shows the behavior of the glint spikes. The target echo signal is relatively small amplitude where the angular error has a spike. This characteristic of glint error will be revisited, since it has an importance on the glint reduction mechanisms.

4.2.3. The relationship between glint and target size

Similar to the discussion in previous sections, smaller targets can be treated as point-like targets when compared to the larger targets. This simple intuitive information about target size is supported by Borden in [13, 14]. An important formula is derived from the Titchmarsh theorem that relates the number of amplitude zeros to the aspect angle of target [14]. Borden presents the following equation,

$$\Delta\eta = \frac{kW}{\pi}\Delta\beta = \frac{2fW}{c}\Delta\beta \tag{4.4}$$

where k is the wave number, W is target width (crossrange extent of target) and β is the aspect angle. This expression states that the number of amplitude fades will increase with increasing target size. This also implies increasing glint error spikes which results in dense glint noise on the average.

Equations 5.12 and 5.30 derived later in Chapter 5 for correlation properties also show the relationship between glint and target extents. The parameters expressed in these equations claim that the correlation of received signals within these derived intervals is inversely proportional to target size. Therefore, target size is an increasing factor for observing glint like signals.

The dependence on target size is simulated with the parameters in Table 4.3. The target's extents in range and crossrange are the same for simplicity. The scattering characteristic of each element is taken random for the same reasons with the previous analysis in this chapter.

Table 4.3 - Simulation configuration of target size effect on glint analysis

Target angle	10deg
Target range	1000m
Random scatterers on target	10
Center Frequency	10GHz
DF Method	Phase monopulse
Simulated minimum target size	1m
Simulated maximum target size	20m
Number of experiments for each size	1000

Figure 4.5 shows the relationship between target size and glint error. Glint error in this case is given as linear error in position for better comparison with the target extent. Although the results in this figure can only show the error for average case, it is important to understand the effect of target size.

The understanding of glint phenomenon points out that the instantaneous behavior of the glint error may be more critical. For this reason the single run simulation for the target size effect is given in Figure 4.6. The errors that go beyond the target extent are marked in this figure to show the importance of glint error.

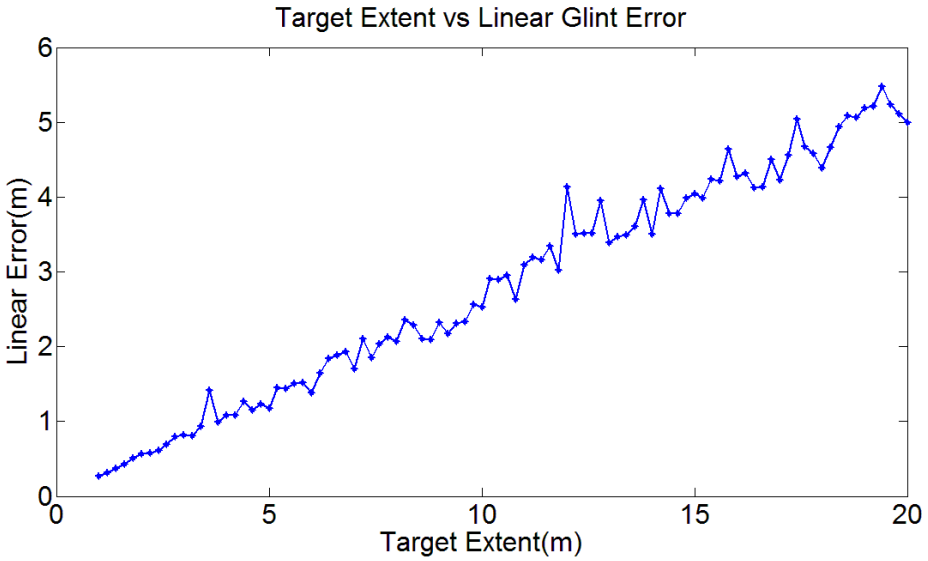

Figure 4.5 - Average target size effect simulation result

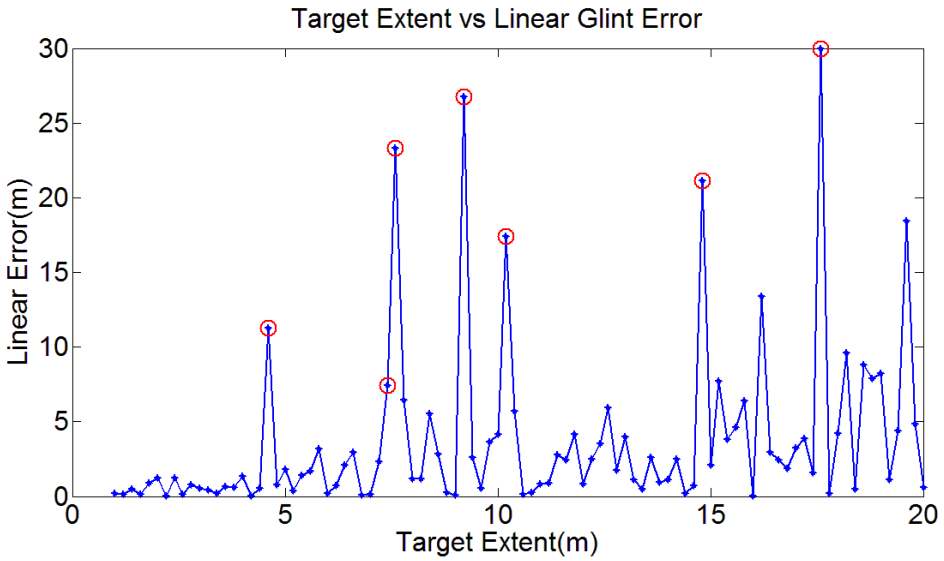

Figure 4.6 - Single run target size effect simulation result

4.2.4. Evaluation of Glint Properties

The characteristics of glint error and signal with glint are important for radar system design and glint reduction mechanisms. These properties should be taken into account by radar engineers.

The importance of glint error is different for different types of systems and different types of targets. For example, if a radar system deals with targets at ranges of 10km or far beyond this, the error due to glint may be negligible when compared with the errors due to radar itself. On the other hand, a homing guided missile radar may be exposed to high glint error levels especially in the terminal phase.

The target type is also important for the radar system. The glint error experienced by homing guided missile for a tank may not be crucial. However the induced glint error by an aircraft carrier may be at high levels that should be accounted for by the radar system.

The negative correlation of target return signal amplitude and the glint error are important for reduction of glint error. If echo amplitude from the target is lower compared to a specified level or to other amplitudes, this measurement may not be taken into consideration or may be considered as a low importance measurement of target information. This idea is the basis of glint reduction mechanisms that will be introduced in next sections.

4.3. Glint Reduction Techniques

Glint phenomenon is a type of noise that is induced by target itself. Therefore, first approach in order to reduce glint error effects may be to use an appropriate filter [14]. However, non-Gaussian characteristic of glint noise makes the filter design problem a difficult task for radar engineer. For this reason, preprocessing for filtering is studied by researchers [15, 16].

Filtering of glint noise may cause loss of the relevant tracking information about the target [14]. Instead of trying to eliminate the glint noise, the approach of producing additional information about target is preferred by the glint reduction researches. As a result, diversity techniques are studied in order to produce additional information about target.

Glint phenomenon, as mentioned earlier, is a result of interfered phase fronts of scattering elements on the target. Glint spike can be eliminated with the use of diversity techniques as they change the complex scattering behavior of individual scatterers.

The diversity techniques listed below are possible methods for glint error reduction in radar systems:

1) Frequency diversity
2) Space or aspect diversity
3) Polarization diversity

In all diversity methods, it is aimed to collect a set of samples which are desired to be uncorrelated [17]. By this way, a selection algorithm can be employed in order to generate more accurate information about the target. The selection algorithms will be discussed in the next section.

Frequency diversity, or frequency agility, employs a number of frequencies in a bandwidth which can be used either simultaneously or in different pulses. The separation of the samples should be able to produce uncorrelated echo signal samples.

For a better understanding of frequency agility, the basic principle of glint should be revisited [14]. Single scatterers cannot produce glint. Thus, increasing the resolution of illumination may resolve multiple scatterers on a complex target. For this reason, a radar system can employ a larger frequency bandwidth to increase the resolution and hence the complex target can be resolved.

Space or aspect diversity is another method that can be used for gathering uncorrelated signal samples to use in glint reduction mechanisms. The basic principle of glint is also applicable for these diversity techniques.

SAR and ISAR imaging concepts are two easy ways to explain the space and aspect diversity techniques, respectively. In SAR imaging, the antenna is moved by the system, so that a synthetic aperture is created. By this way, the resolution of radar system is increased. Space diversity can also be explained by this concept, since increasing resolution will result in resolving the targets better.

On the other hand, in ISAR imaging, the target is allowed to change its aspect and a synthetic aperture is generated by illuminating target many times. Aspect diversity technique also uses this concept to increase the resolution, so that the glint error will be reduced.

At this point, illustration of the glint spike change for different frequencies and aspects will be helpful in understanding the underlying concepts. The glint error is simulated for a target which extends 5m in both range and crossrange. Target consists of 10 scattering elements and the geometric center of the target is at an angle of 10°. Phase monopulse is used for reference angle generation.

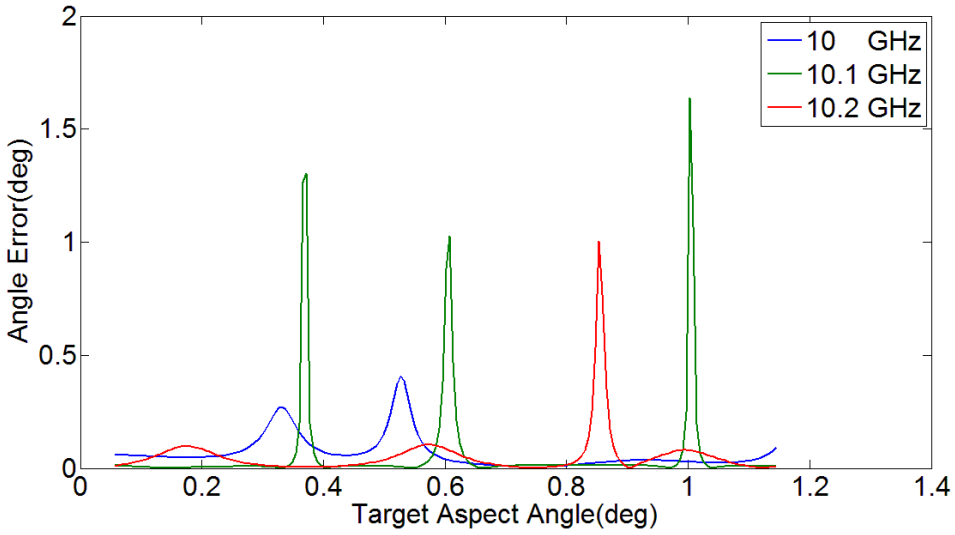

Figure 4.7 - Angular glint error for different frequencies and aspects

Figure 4.7 illustrates the motivation in the use of diversity techniques, since the glint spikes are changing due to either a frequency change or an aspect change. The data from diverse measurements shown above may be assembled in order to improve information about target.

Polarization diversity is another method that can be used to change the scattering characteristics of different elements on target. In this method, it is expected that each scattering center has different scattering properties for different polarizations. Therefore, the effectiveness of polarization diversity is dependent on the polarization characteristics of each element [17].

Diversity methods provide considerable improvements as various researchers have shown theoretically. Frequency diversity is the most promising method among these diversity techniques. However, bandwidth requirement of frequency diversity may

not be realizable for some radar platforms. In this case, space or aspect diversity is the second possible best choice for glint mitigation purposes. Polarization diversity has more limitations than other methods, since fully polarized systems are much more expensive than ordinary systems [14]. Therefore, frequency and spatial diversity methods are investigated in this thesis. Theoretical consideration related to these techniques and the simulation results are given in the next chapter.

Diversity techniques need selection mechanisms that will make use of the generated information to reduce the glint error. These mechanisms are the object of the next section.

4.3.1. Diversity Selection Methods

Diversity selection methods are mostly based on the concept of negative correlation of glint error and the echo amplitude. Several weighting mechanisms can be applied in order to assemble a number of samples provided by diversity techniques. The weighting mechanism is applied on the target angle measurements. The output of the weighting for N samples can be expressed by the following:

$$\theta_{out} = \frac{\sum w_k \theta_k}{\sum w_k}, \qquad k = 1..N \tag{4.5}$$

The weighting scheme can be a simple averaging. However, an averaging that uses the signal levels returned from the target should be more suitable for glint reduction. There can be different weighting mechanisms for sure, but the weighting functions that are listed below are evaluated in this study.

- Mean weighting
- Linear weighting
- Square weighting
- Largest amplitude selection
- Rank detector

Among the above selection methods, rank detector is advised by Guest [18] for glint reduction by detecting the glint spikes. However, the weighting scheme used here is somewhat different in the sense of using guards and windows. Rank detector used here is using all of the samples in comparison process.

The weights for each selection method are formulated below:

- Mean weighting

$$w_k = 1 \tag{4.6}$$

- Linear weighting

$$w_k = |E_k| \tag{4.7}$$

- Square weighting

$$w_k = |E_k|^2 \tag{4.8}$$

- Largest amplitude selection

$$w_k = \begin{cases} 1\,, & for\ \{(k) \mid |E_k| = \max(|\bar{E}|)\} \\ 0\,, & otherwise \end{cases} \tag{4.9}$$

- Rank detector

$$w_k = \sum_{n=1}^{n=N} rank_{k,n} \tag{4.10}$$

$$rank_{k,n} = \begin{cases} 1\,, & if\ |E_k| > |E_n| \\ 0\,, & if\ |E_k| \leq |E_n| \end{cases} \tag{4.11}$$

General performance of these methods is illustrated for random targets with random scatterings in Figure 4.8. The below configuration in Table 4.4 is used for this purpose. 20 samples for each target will be the input of selection methods in this analysis.

Table 4.4 - Simulation configuration of diversity selection method analysis

Target depth	5m
Target width	5m
Target angle	10deg
Target range	1000m
Random scatterers on target	10
Center Frequency	10GHz
DF Method	Phase monopulse
Number of random scattering for each target	20
Number of experiment	10

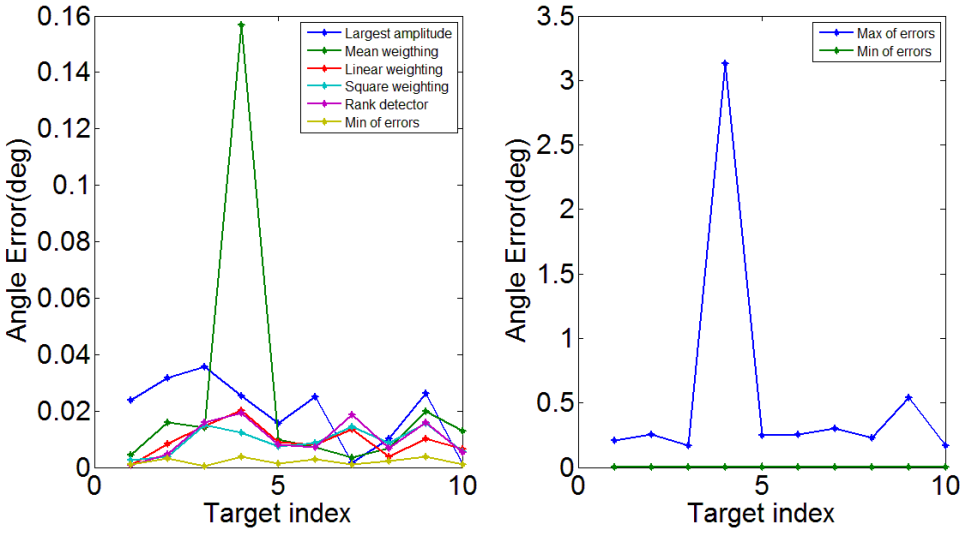

Figure 4.8 - Glint error reduction with selection methods

The reduction results of the described simulation are given in Figure 4.8. All methods other than the mean weighting can make use of the negative correlation property. Besides that, the largest amplitude selection method may create erroneous results. Rest of the methods generates considerably good reduction results.

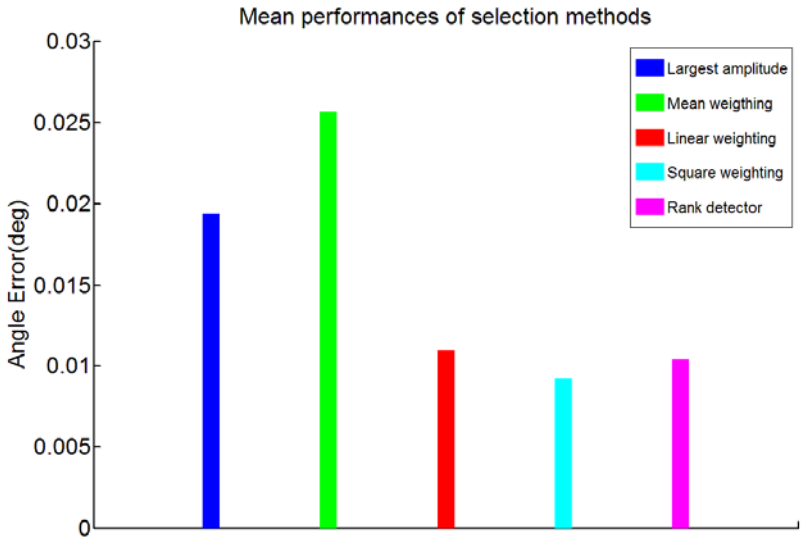

Figure 4.9 – Mean glint error levels for different selection methods

Mean performance of the selection methods are compared in Figure 4.9 with a long run of simulation for 10000 random targets. The parameters other than “Number of experiment” in the simulation configuration are the same.

The mean error values in Figure 4.9 show that the square weighting method is the best one of evaluated methods. Nevertheless, the linear weighting method and the rank detector method may be alternative methods with their low level of angular glint errors.

CHAPTER 5

GLINT REDUCTION ANALYSIS

5.1. Frequency Diversity

Frequency diversity, in other words frequency agility, is one of the techniques used for reducing radar pointing errors. Glint error due to fluctuation of target return signal may be reduced by using different frequencies and this section investigates the frequency diversity. Sampled target signal at different frequencies used with diversity selection methods can give better angle and range information about the target.

Among the diversity methods, frequency diversity is regarded to be relatively more outstanding. Frequency diversity is an initial step to reduce tracking errors due to target glint. In the literature, several methods are proposed in order to utilize the frequency diversity by various researchers [19, 20, 22, and 23]. With this motivation, frequency diversity to reduce glint error is examined from certain perspectives in detail in this chapter.

In this chapter, statistical properties of the return signal with frequency agility will be given.

- The autocorrelation function of the return signal will be found following Birkemeier and Wallace [21].
- The critical frequency change will be found and its effect will be investigated [19, 21].

After investigating the statistical properties related with frequency agility, improvements with diverse frequencies will be analyzed.

- An approximate improvement factor with frequency agility will be introduced following Lind [20].
- Simulations for diverse frequencies will be made and diversity selection methods will be used for reducing angular pointing errors. Evaluation of selection methods will be given in a comparative manner.
- Effects of frequency agility parameters such as frequency bandwidth, sample of different frequencies and choice of frequencies in the specified bandwidth will be discussed.

Studying on the statistical properties and advantages of the frequency agility, several questions will be answered concerning the implementation of frequency diversity method. These questions can be summarized as follows:

- What numbers of frequency samples are needed?
- What is the effect of bandwidth on reduction?
- How does the frequency sequence affect the reduction?
- Which diversity selection method is more effective compared to others?

In order to answer the above questions, MATLAB simulations which uses return signal from an extended target have been conducted. The output data from the simulation are used to explain the properties of a frequency agile system.

5.1.1. Autocorrelation Function of Frequency Agile Signals

Understanding the autocorrelation will provide an insight on the sample characteristic. Thus, sampling of the echo signal can be made properly for efficient reduction of glint.

The derivations given here are based on the model of Birkemeier and Wallace [21]. The target model for the derivation is the basic line target but it is time frozen. This is done in order to show more representative frequency dependency of the autocorrelation function. Target orientation angle with respect to the radar is also frozen at θ_0. Target length is L and is located at range r_0. The geometry of the model is given in Figure 5.1.

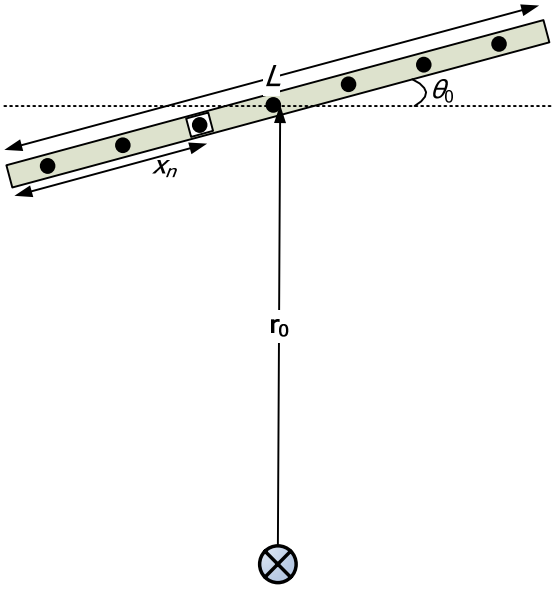

Figure 5.1 - Target geometry for autocorrelation function

Let the return signal be $y(f)$, then

$$y(f) = \sum_n a_n e^{j(2\pi f \frac{2r_n}{c} + \phi_n)} \tag{5.1}$$

a_n : $Amplitude\ of\ the\ return\ from\ n\text{th}\ scatterer$

ϕ_n : $Phase\ of\ the\ return\ from\ n\text{th}\ scatterer$

r_n : $Range\ of\ the\ n\text{th}\ scatterer$

- Phase angles, $\phi_n's$, are independent and uniformly distributed from 0 to 2π.
- r_n can be taken as $r_0 + x_n * \sin(\theta_0)$

The autocorrelation function can be formulated as:

$$R(\Delta f) = E\{y(f) * y^*(f + \Delta f)\} \tag{5.2}$$

$$R(\Delta f) = E\left\{\sum_n a_n e^{j(2\pi f \frac{2r_n}{c} + \phi_n)} \sum_m a_m e^{-j(2\pi (f+\Delta f) \frac{2r_m}{c} + \phi_m)}\right\} \tag{5.3}$$

$$R(\Delta f) = \sum_n \sum_m E\{a_n a_m\} e^{j\left(2\pi f \frac{2(r_n - r_m)}{c}\right)} e^{-j\left(2\pi \Delta f \frac{2r_m}{c}\right)} E\{e^{j(\phi_n - \phi_m)}\} \quad (5.4)$$

Expected values of the random variables, amplitude and phase angle, are

$$E\{e^{j(\phi_n - \phi_m)}\} = \begin{cases} E\{e^{j\phi_n}\} E\{e^{j\phi_m}\} = 0 \ , & n \neq m \\ E\{e^{j0}\} = 1 \ , & n = m \end{cases} \quad (5.5)$$

$$E\{a_n a_m\} = \mu_a{}^2 \qquad for \ \ n = m \quad (5.6)$$

Thus, autocorrelation function reduces to:

$$R(\Delta f) = \mu_a{}^2 \sum_n e^{-j\left(2\pi \Delta f \frac{2(r_0 + x_n * \sin(\theta_0))}{c}\right)} \quad (5.7)$$

$$R(\Delta f) = \mu_a{}^2 e^{-j\left(2\pi \Delta f \frac{2r_0}{c}\right)} \sum_n e^{-j\left(2\pi \Delta f \frac{2\, x_n * \sin(\theta_0)}{c}\right)} \quad (5.8)$$

Summation in the above equation can be interpreted as integration over x which is the distance from the middle of target. This makes the line target composed of infinite scatterers.

$$\int_{-L/2}^{L/2} e^{-j\left(2\pi \Delta f \frac{2\, x * \sin(\theta_0)}{c}\right)} dx = \left. \frac{e^{-j\left(2\pi \Delta f \frac{2\, x * \sin(\theta_0)}{c}\right)}}{-j\left(2\pi \Delta f \frac{2\ * \sin(\theta_0)}{c}\right)} \right|_{-L/2}^{L/2} = \frac{\sin(2\pi \Delta f \frac{L \sin(\theta_0)}{c})}{2\pi \Delta f \frac{\sin(\theta_0)}{c}} \quad (5.9)$$

Finally, the autocorrelation function can be expressed as:

$$R(\Delta f) = \mu_a{}^2 e^{-j\left(2\pi \Delta f \frac{2r_0}{c}\right)} \frac{\sin(2\pi \Delta f \frac{L \sin(\theta_0)}{c})}{2\pi \Delta f \frac{\sin(\theta_0)}{c}} \quad (5.10)$$

Consequently, autocorrelation function is expressed in a compact form for a simple target geometry. The sinc structure in the autocorrelation may create uncorrelated target signals for higher frequency differences. Therefore frequency difference, Δf, has importance on the glint error with frequency agility.

Next section of this chapter investigates the autocorrelation function and the effects of this frequency difference.

5.1.2. Critical Frequency Change

The properties of autocorrelation function are examined in order to understand the signal properties of return signal with frequency agility. The period of exponential term is greater than the sinusoidal term. Thus, the envelope is enough to consider since target range, r_0, is much greater than the extent of the target. The envelope of autocorrelation function which follows a sinc structure is given by:

$$|R(\Delta f)| = \frac{\sin\left(2\pi\Delta f \frac{L\sin(\theta_0)}{c}\right)}{2\pi\Delta f \frac{\sin(\theta_0)}{c}} \tag{5.11}$$

The illustration of this envelope is important for the derivation of critical frequency change. Therefore, an example of autocorrelation function is given in Figure 5.2 for a target length of 1 meter and orientation angle of 90^0. The autocorrelation function envelope is given for a bandwidth of 1GHz.

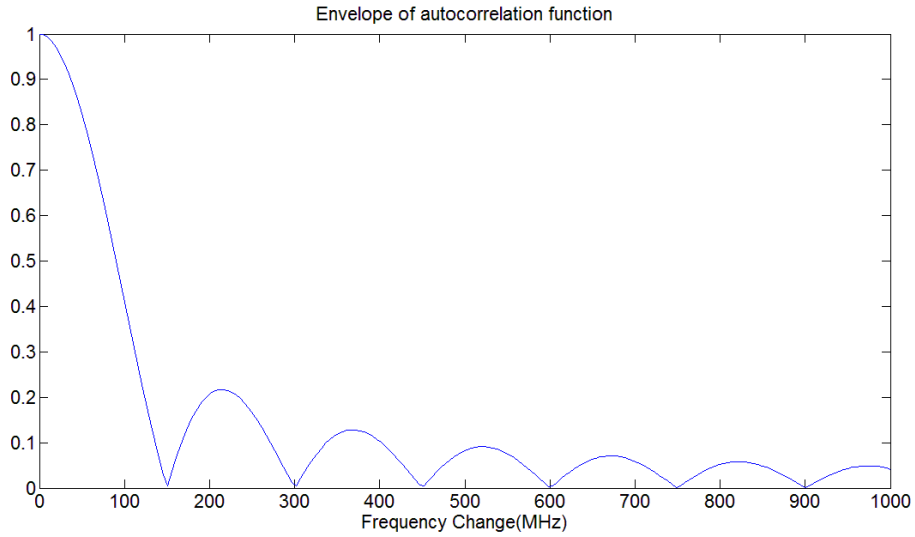

Figure 5.2 - Example of target signal's autocorrelation envelope for frequency change

Figure 5.2 shows that two pulses can be treated as decorrelated for a certain frequency difference. This frequency difference, the critical frequency change, Δf_c, is found from the first zero of the autocorrelation envelope.

$$\Delta f_c = \frac{c}{2L\sin(\theta_0)} = \frac{c}{2D}, \qquad where\ D = L\sin(\theta_0)\ is\ the\ target\ depth \tag{5.12}$$

Although large targets produces more glint induced angle tracking error, the above equation shows that the increasing target depth can supply more uncorrelated sample in a fixed bandwidth. Thus, efficient sampling is important to reduce the higher glint error for larger targets.

5.1.3. Improvement with Frequency Agility

In this section of the chapter, an approximate improvement factor will be presented following the results of Lind [20]. Then frequency agility method will be applied to the simulation environment.

Firstly improvement factor defined by Lind can be derived with the below steps:

$$S_{FF} = \frac{G}{B_G} \tag{5.13}$$

$$S_{FA} = P_C S_{FF} + (1 - P_C)\frac{2G}{f_p} \tag{5.14}$$

$S_{FF} : Spectral\ density\ of\ glint\ with\ fixed\ frequency$

$G : Glint\ power$

$B_G = Glint\ bandwidth$

$S_{FA} : Spectral\ density\ of\ glint\ with\ frequency\ agility$

$P_C = Probability\ of\ undercritical\ frequency\ jump$

$f_p = Pulse\ repetition\ frequency$

Since the spectral density are measure of powers, the improvement factor is expressed as

$$I = \sqrt{\frac{S_{FF}}{S_{FA}}} \tag{5.15}$$

There is a probability that the frequency jump of frequency agility may not be enough for decorrelation of two pulses. This is the probability of undercritical frequency jump and can be expressed as

$$P_C = \frac{2\Delta f_c}{B_{FA}} \tag{5.16}$$

where B_{FA} is the bandwidth of frequency agility and Δf_c is the previously found critical frequency difference. P_C can also be expressed as

$$P_C = \frac{2 * (\mathrm{c}/2\mathrm{D})}{B_{FA}} = \frac{c}{DB_{FA}} = \frac{\lambda_{FA}}{D} \tag{5.17}$$

λ_{FA} : $Frequency\ agility\ wavelength = \frac{c}{B_{FA}}$

At typical radar frequencies, $P_C \ll 1$, and we may assume that $1 - P_C = 1$. Therefore, S_{FA} and the improvement factor can be expressed as:

$$S_{FA} = \frac{\lambda_{FA}}{D} S_{FF} + \frac{2G}{f_p} \tag{5.18}$$

$$I^2 = \frac{S_{FF}}{S_{FA}} = \frac{1}{\frac{1}{D/\lambda_{FA}} + \frac{1}{f_p/2B_G}} \tag{5.19}$$

As a result, the improvement factor can be approximated by

$$I^2 = \begin{cases} \frac{f_p}{2B_G}, & if \ \ f_p/2B_G \ll D/\lambda_{FA} \\ \frac{D}{\lambda_{FA}}, & if \ \ D/\lambda_{FA} \ll f_p/2B_G \end{cases} \tag{5.20}$$

This result can be interpreted such that the square of improvement factor is the smallest of the two ratios above. Generally the smallest one is the latter, and it determines the improvement for frequency diversity. Thus, the frequency agility bandwidth is an important factor and improvement is proportional to the square root of this bandwidth.

$$I \propto \sqrt{B_{FA}} \tag{5.21}$$

An approximate improvement table can be given using Equation 5.20. The improvements are given in Table 5.1 for the latter ratio in Equation 5.20.

Table 5.1 - Approximate improvement with frequency diversity

Improvement factor table		Frequency Agility Bandwidth(MHz)		
		200	*500*	*1000*
Target Depth(m)	*2*	1.15	1.83	2.58
	5	1.83	2.89	4.08
	10	2.58	4.08	5.77

Thus one can expect that 500MHz bandwidth is required for a 5 meter target extending in range in order to reduce glint error by a factor of 3. Nevertheless, this table can only give an intuition to a rough improvement estimate but may be helpful in the design of frequency agile radar system.

5.1.4. Simulation Results of Frequency Agility

Target model for frequency agility processing is composed of fixed number of point scattering elements. The positions of scatterers are random within a rectangular region. Therefore the phase of scatterers could be considered as randomly distributed for the signal model used in this chapter for the derivation of autocorrelation function. Furthermore all scatterers have the same amplitude in the simulation, which is enough for the model [11].

The analyses are made up by setting the parameters like the frequency agility bandwidth, the number of samples. The target dimension is also changed to see the relationship between the frequency agility bandwidth with target extent. Target dimension is known to be an increasing factor on glint from Chapter 4, so the frequency agility effect on the glint of larger targets should be investigated. The parameter effects will be presented with the outputs of Monte Carlo simulations. Selection methods for signal processing will also be under examination.

5.1.4.1. Effect of Sample Number in a Fixed Bandwidth

The target echo cannot be sampled at higher number or at desired frequencies due to the limitations of the radar system which can be both hardware and software

related. If the system needs a large number of samples, system may not be able to serve intensive processing requirements of these samples. Therefore, sample number should be at acceptable levels for processing.

This section of the simulation results aims to develop an insight for choosing sample number or frequency interval of samples. Table 5.2 shows the simulation configuration which is used to illustrate the importance of the frequency spacing of the samples.

Table 5.2 - Simulation configuration of sample number analysis

	Target 1	**Target 2**
Target depth	5m	1m
Target width	5m	1m
Target angle	30deg	
Target range	1000m	
Random scatterers on target	10	
Frequency agility bandwidth	100MHz 500MHz	100MHz 500MHz 1000MHz
Frequency spacing regime	Linear	
Maximum number of samples	20	
Starting Frequency	9GHz	
DF Method	Phase Monopulse	
Number of experiments	1000	

Simulation results for Target 1 are given below in Figure 5.3 and Figure 5.4. Sampled target return signal at different frequencies are combined with the selection algorithms which are mentioned before in Chapter 4. In this target configuration, we expect the return signal to be decorrelated when the frequency difference is 30MHz. Although a bandwidth of 100MHz will be enough for acquiring uncorrelated samples,

only a few samples taken can be uncorrelated. Therefore, getting more samples in this relatively small bandwidth will not affect the reduction much.

Figure 5.3 shows that 4 or 5 samples are enough for a target depth of 5m and 100MHz bandwidth. After this sufficient number of samples, it can be said that glint error becomes steady at an achievable level for each selection method. Square weighting seems to be the most appropriate selection method for this target and frequency agility configuration. However, there is a slight increase in the pointing error for square weighting, linear weighting and rank detector methods with unnecessarily taken samples.

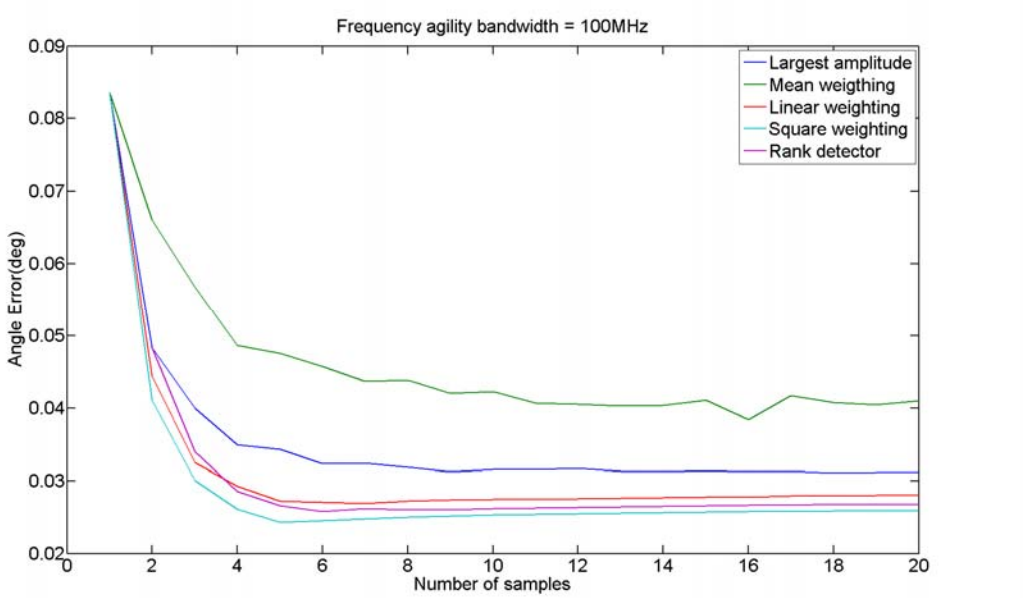

Figure 5.3 - Target 1 simulation results for 100MHz bandwidth

Figure 5.4 shows that glint error is decreasing with increasing number of samples in 500MHz bandwidth. In this configuration, getting more samples becomes important in this fixed bandwidth. This can be easily understood when the ratio of bandwidth and critical frequency difference ratio is considered. This ratio is theoretically 500/30 while the ratio of previous configuration is 100/30. Obtaining a higher ratio could be interpreted such that gathering more samples will be more advantageous.

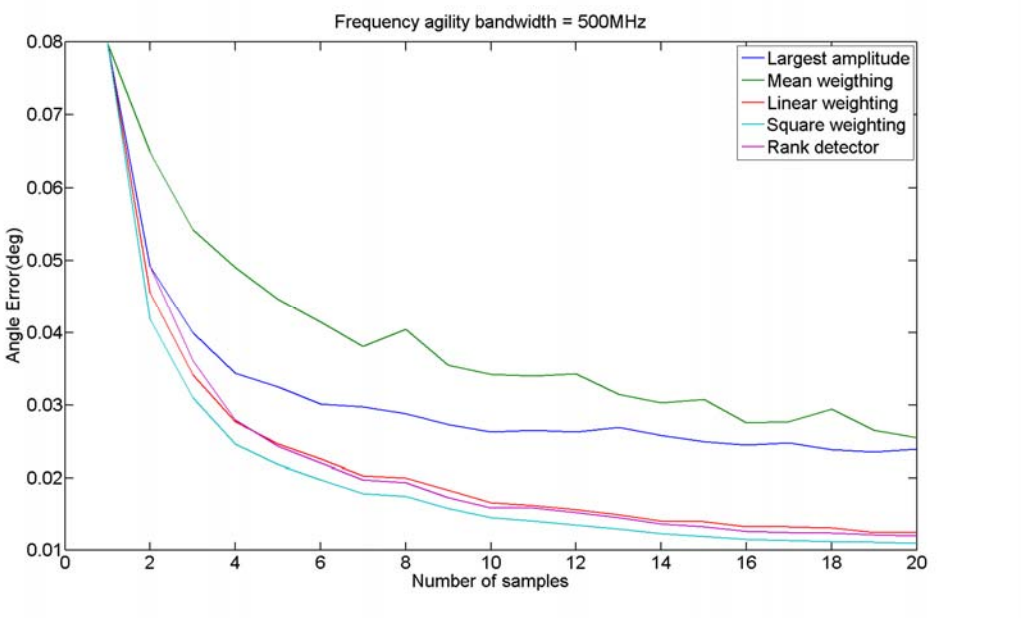

Figure 5.4 - Target 1 simulation results for 500MHz bandwidth

The frequency spacing of samples is 25MHz for 20 samples. Thus, all samples taken can be considered as uncorrelated. By this way, correction of the measurements with selection algorithms can produce more accurate target angle estimates. For this satisfactory bandwidth, the most suitable selection algorithm is again the square weighting method. Though, the linear weighting method and the rank detector method can be considered as equally effective on the reduction of glint error.

Simulation results for Target 2 are given below in Figure 5.5 and Figure 5.6. In this target configuration we expect the return signal to be decorrelated when the frequency difference is 150MHz. Thus, 100 MHz bandwidth is not suitable for sufficiently uncorrelated samples.

Maximum frequency difference will be 100 MHz for 2 sample case. Other cases will provide more correlated samples. Therefore, those samples may introduce extra error in the mean. Figure 5.5 shows the reduction result for 100 MHz frequency agility bandwidth. The error increases for sample numbers greater than 3.

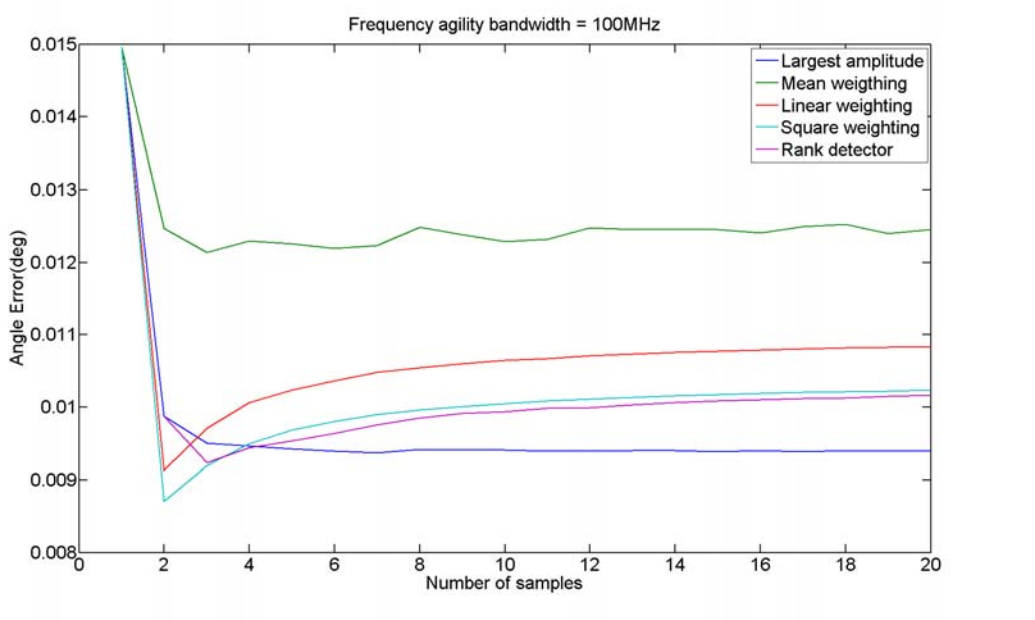

Figure 5.5 - Target 2 simulation results for 100MHz bandwidth

The most successful method in this insufficient bandwidth is the largest amplitude selection method. Linear and square weighting methods and rank detector method lose their superiority on largest amplitude method. Nonetheless, they are still advantageous up to 3 samples which can be considered as generating relatively uncorrelated samples. The bandwidth to critical frequency change ratio is 100/150 for this target and bandwidth settings. As mentioned earlier, this ratio should be greater for higher glint error reduction. However, a ratio which is smaller than unity makes the frequency agility useless. When we consider increasing this ratio to 500/150 and 1000/150 by setting bandwidth to 500MHz and 1000MHz, frequency agility uses the samples more effectively.

Firstly, for 500MHz bandwidth, a few uncorrelated samples can be taken. With increasing sample number, the frequency difference between samples will be getting smaller than critical frequency change. The reduction results shown in Figure 5.6 also agree with the above considerations. After 5 samples, the selection methods do not improve angle estimations and the angle error becomes steady. When we compare the selection methods, it is seen that square weighting is again the most suitable method. This of course is due to sampling in a sufficient bandwidth.

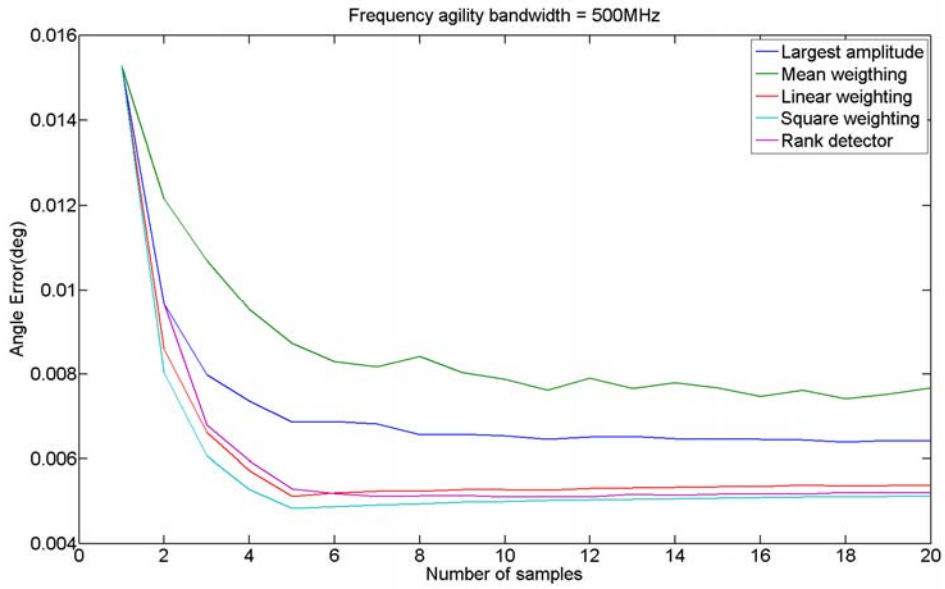

Figure 5.6 - Target 2 simulation results for 500MHz bandwidth

Secondly, for 1000MHz bandwidth, more uncorrelated samples can be gathered. This makes the angle error reach its steady level for larger number of samples. In this bandwidth, it becomes more beneficial to sample the target return signal at a greater number of points. The simulation results can be seen in Figure 5.7.

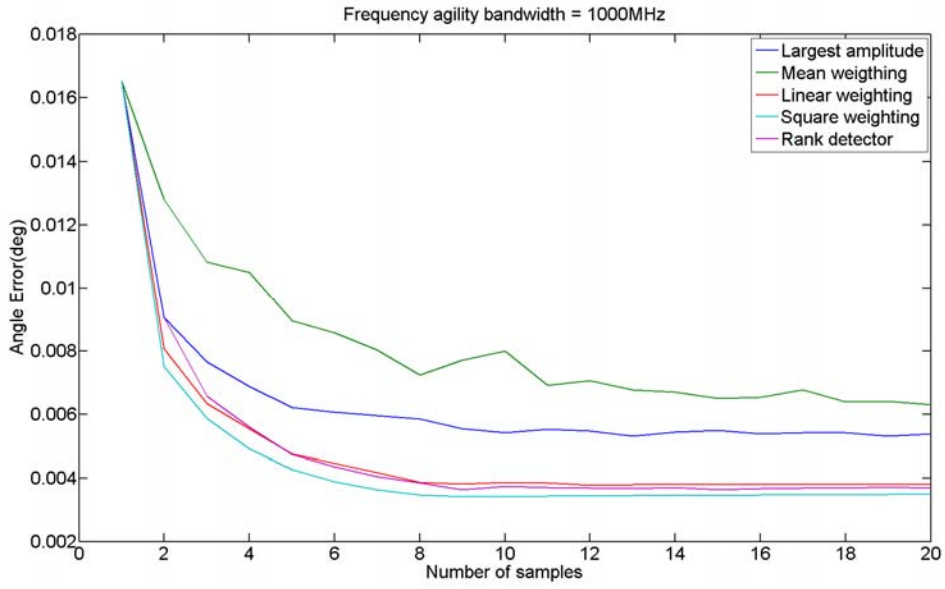

Figure 5.7 - Target 2 simulation results for 1000MHz bandwidth

5.1.4.2. Effect of Agility Bandwidth for Fixed Number of Samples

Frequency agility bandwidth is known to be a positive factor in glint reduction. However, radar systems have limited bandwidths due to various reasons like cost, physical size or capability of hardware units. Thus, effective usage of bandwidth should be investigated. If a radar system employs frequency agility to measure target angle more precisely, then the system must be able to utilize reduction algorithms at full capacity. Therefore, this part of the frequency diversity simulations investigates the effective usage of the bandwidth.

The below simulation configuration in Table 5.3 is used to illustrate the importance of the frequency diversity bandwidth.

Table 5.3 - Simulation configuration of frequency agility bandwidth analysis

	Target 1	**Target 2**
Target depth	5m	1m
Target width	5m	1m
Target angle	30deg	
Target range	1000m	
Random scatterers on target	10	
Sample number	10 samples 30 samples	
Frequency spacing regime	Linear	
Maximum bandwidth	1000MHz	
Diversity Selection Method	Square weighting	
Starting Frequency	9GHz	
DF Method	Phase Monopulse	
Number of experiments	1000	

Simulation results for Target 1 are given below in Figure 5.8 and Figure 5.9. Square weighting method is used to process the samples for error reduction. The results are

compared with the approximate improvement factor which is given before in this chapter.

The improvement factor was given in Equation 5.21 as proportional to square root of the bandwidth. The theoretical angle error line represents the expected error with the improvement factor. Theoretical line is calculated using the reciprocal of bandwidth square root. This can be formulated as $e_t = e_i/\sqrt{B_{FA}}$, where e_t is error in theory and e_i is an initial error. In the simulation results, e_i is taken as the angle error result for the first bandwidth used.

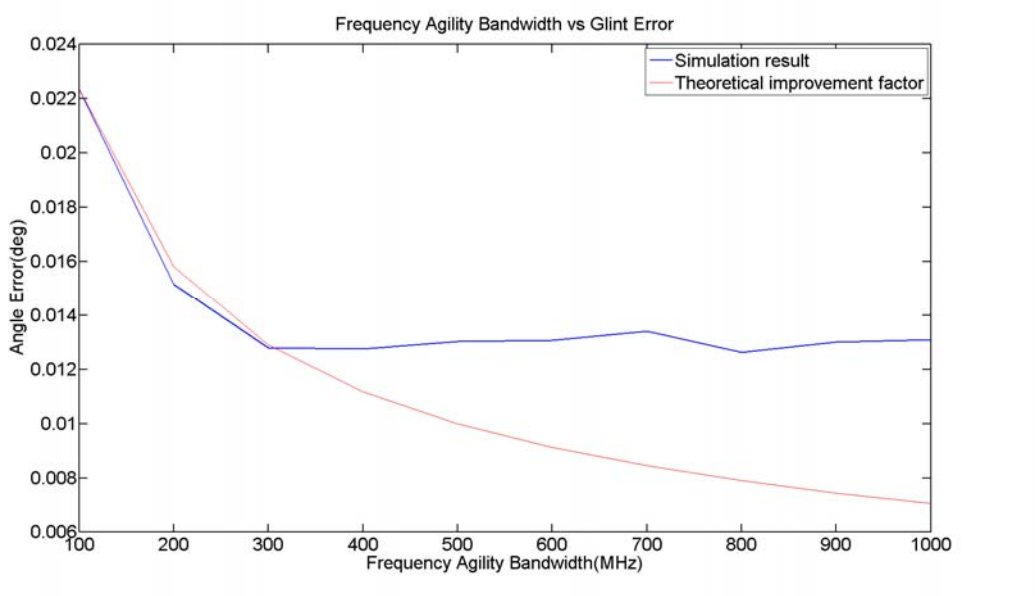

Figure 5.8 - Target 1 simulation results for 10 samples in bandwidth

Firstly, 10 samples case is given in Figure 5.8. The figure shows that the frequency agility cannot reduce glint error after 300MHz bandwidth. At this point the critical frequency difference for Target 1 which is 30MHz becomes important. For 300MHz bandwidth, 10 samples make the frequency spacing between samples 30MHz. Thus, the samples can be treated as uncorrelated and all of the samples will contribute the reduction process. After 300MHz bandwidth, 10 samples will be again uncorrelated; nevertheless more uncorrelated samples can be taken for higher bandwidth. Thus, 10 samples are not enough to utilize the bandwidth fully and the glint error remains steady after 300MHz for this simulation configuration.

Secondly, 30 samples are taken for effective use of high diversity bandwidths. The reduction results are given in Figure 5.9. The results show that high bandwidths require more samples to reach higher reduction rates. Actually, the spacing of samples and the critical frequency change relation determines the efficiency of frequency diversity.

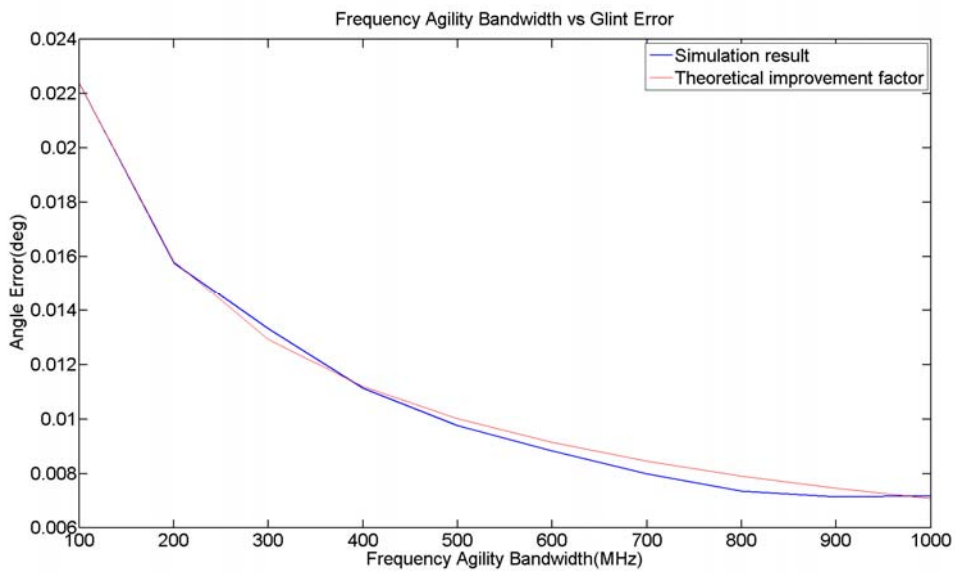

Figure 5.9 - Target 1 simulation results for 30 samples in bandwidth

At this point, a ratio will be introduced to estimate the total performance of frequency agility better. The below ratio can be regarded as an important factor that influence the total performance of frequency agility. Let this performance factor be

$$p_f = \frac{s_s}{\Delta f_c} \tag{5.22}$$

where s_s is the sample spacing and Δf_c is the critical frequency difference. This factor can be interpreted for different intervals as:

1) If $p_f > 1$, bandwidth cannot be used efficiently.
   - Number of samples may be increased to decrease p_f.
2) If $p_f < 1$, number of samples in the band is unnecessarily high.
   - Processing capacity of the system can be enhanced.

3) If $p_f \ll 1$, frequency agility cannot reach the maximum improvement level.
   - Correlation of samples can be broken by increasing the frequency spacing.

Therefore, the second choice will be a better way to use frequency agility. Radar systems which can provide extra processing capabilities have the chance to employ more beneficial frequency agile unit.

After examining a relatively large target with fixed sample number, a small target is examined. The simulation results for Target 2 are given below in Figure 5.10 and Figure 5.11. Target 2 has a critical frequency difference value of 150MHz.

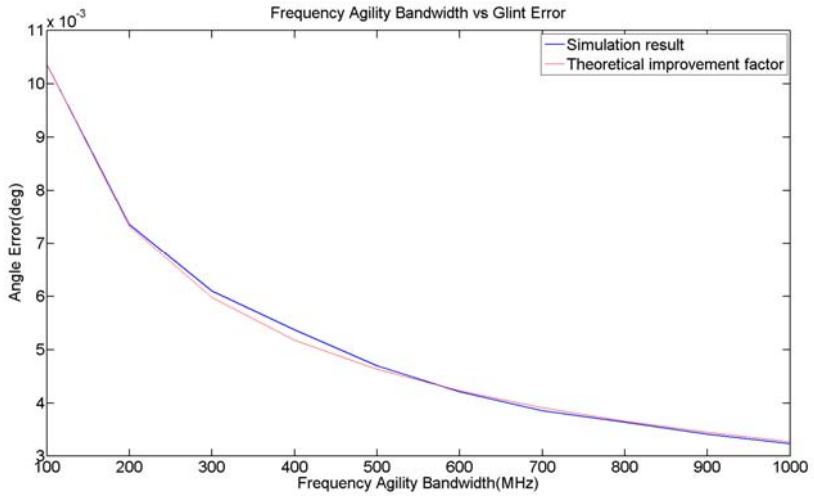

Figure 5.10 - Target 2 simulation results for 10 samples in bandwidth

Firstly, 10 samples case is given in Figure 5.10. Performance factor introduced above is increasing from 0.133 to 0.667 for this target and sampling configuration. Therefore, we can say that this configuration falls in the second interval. Although we sampled the frequency bandwidth unnecessarily, the improvement with frequency diversity is attained.

Secondly, 30 samples case is given in Figure 5.11. Performance factor is increasing from 0.044 to 0.222 for this target and sampling configuration. As a result this configuration can be considered in third interval for lower bandwidths and in second interval for higher bandwidths. Therefore, glint error suffers a separation from

theoretical error line for lower bandwidths. However, simulation results reach the theoretical line for higher bandwidths when the performance factor moves to the second region.

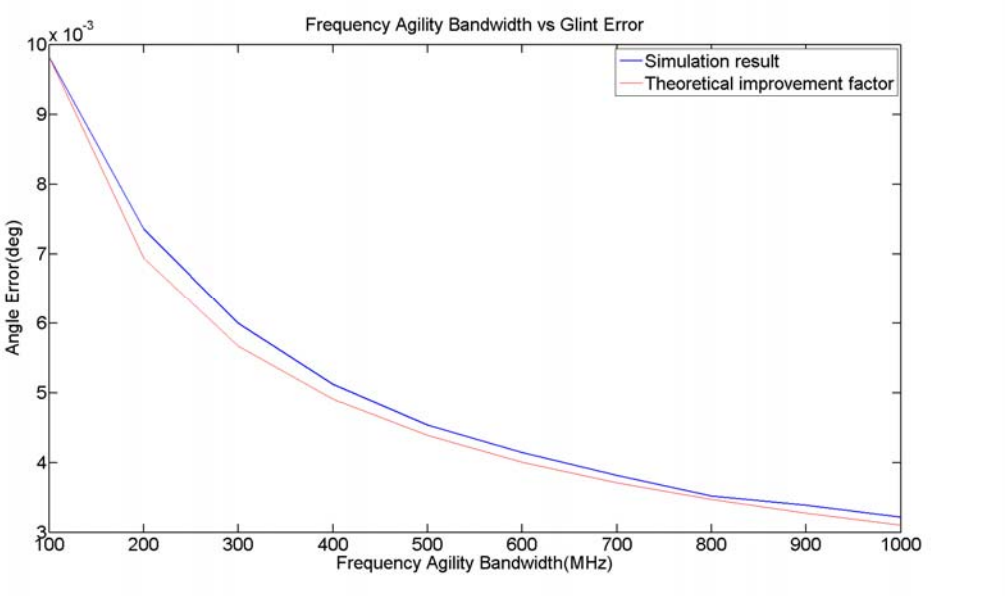

Figure 5.11 - Target 2 simulation results for 30 samples in bandwidth

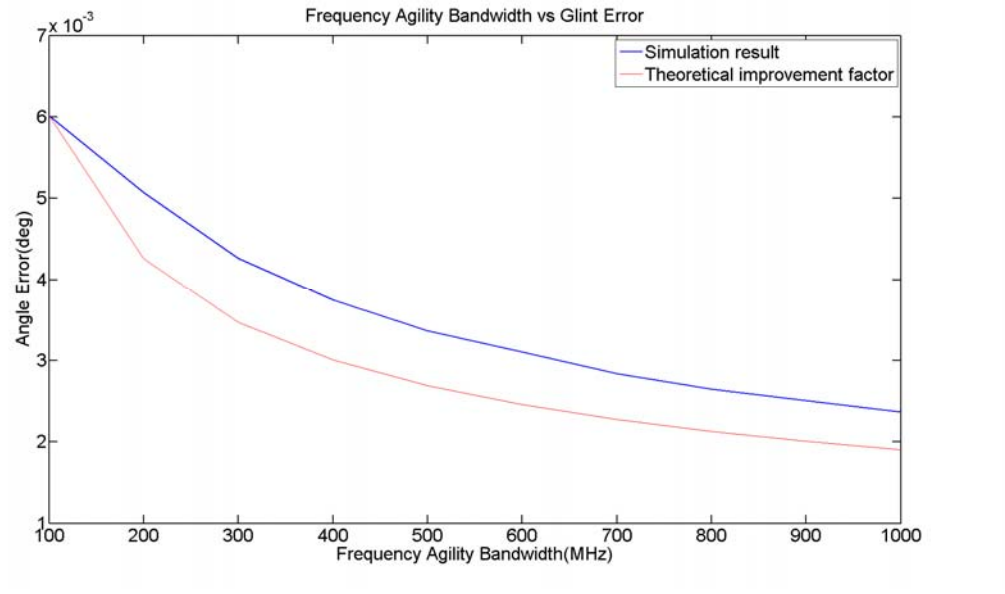

Figure 5.12 - Simulation results for 50 samples in bandwidth for target of 0.5m extending in range and crossrange

An extra simulation is made for a target of 0.5m depth and width. 50 samples are taken in a maximum bandwidth of 1GHz. This simulation shows the worst case for the performance factor. Performance factor is increasing from 0.013 to 0.066 for this target and sampling configuration. As a result, the error line of simulation cannot reach the theoretical error line for all bandwidths used in the simulation. Simulation results are given in Figure 5.12.

5.1.4.3. Frequency Spacing Regime Effect on Reduction

Spacing of samples is important for the return signal statistics. Linearly spaced samples are used in the simulations up to this part of the chapter. This part aims to examine the effect of random spacing of samples in the bandwidth. Thus, the below simulation configuration in Table 5.4 is used for this purpose. The simulation parameters cannot be broadened to higher bandwidths or higher number of runs because of the high processing and memory requirements of the MATLAB program.

Table 5.4 - Simulation configuration of sample spacing regime

Target depth	5m	
Target width	5m	
Target angle	30deg	
Target range	1000m	
Random scatterers on target	10	
Sample number	20 samples	
Frequency spacing regime	Linear	Random
Maximum bandwidth	700MHz	
Diversity Selection Method	Square weighting	
Starting Frequency	9GHz	
DF Method	Phase Monopulse	

50 Monte Carlo simulations are used in order to figure out the average performance of the random spacing of samples in the bandwidth.

Although random spacing cannot guarantee the uncorrelated samples, it may provide samples with lower angle error. The reduction results at 700MHz bandwidth are presented for all averaging methods in Figure 5.13. Although the diversity selection methods produce smoother reduction results for random spacing regime, the linear spacing regime can still mitigate the glint error better. The square weighting method is also the best averaging algorithm for random spacing of samples in the frequency agility bandwidth.

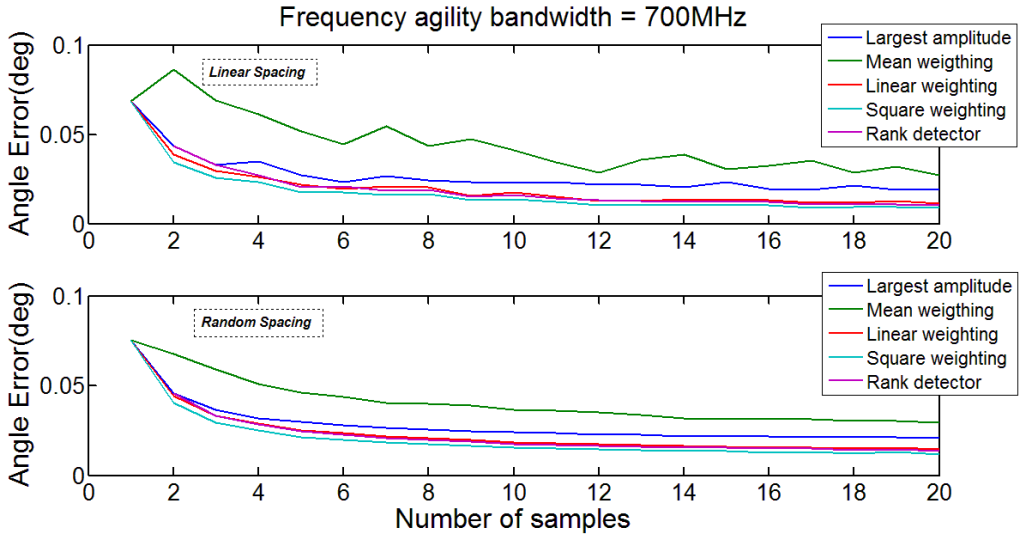

Figure 5.13 - Sample number effect in both spacing regime

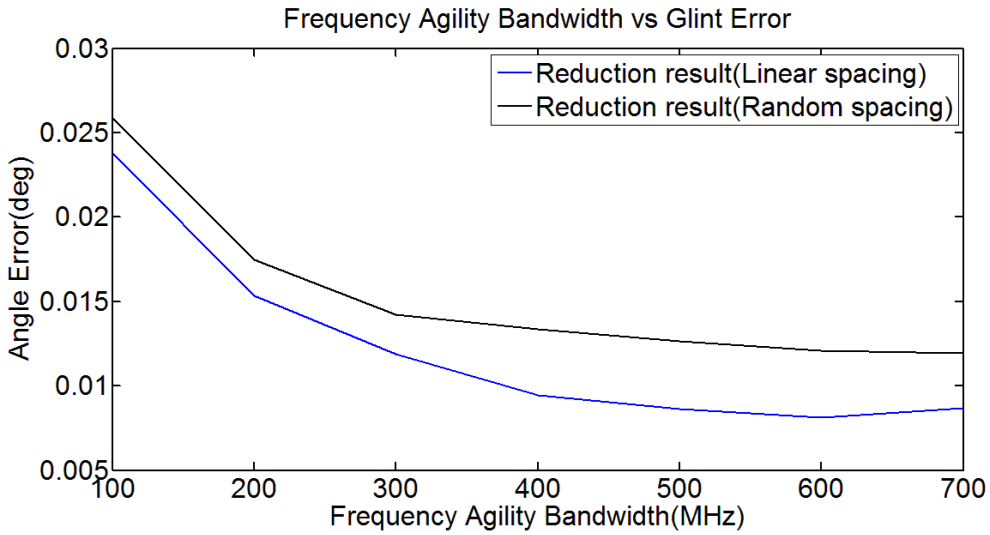

Figure 5.14 - Frequency agility bandwidth effect for both spacing regime

Figure 5.14 shows the reduction results with random spacing. The square weighting method is used as the diversity selection method since it gives better results than the other methods. The glint error with averaging methods is smaller for linear spacing regime in all agility bandwidths.

5.2. Spatial Diversity

Space or aspect diversity, i.e. spatial diversity, is another technique that can be employed in radar systems for glint mitigation. Space diversity can easily be understood by considering the main reason of glint.

The main reason of glint was the phase interference of different scatterers on the target. Thus, glint induced by the target can be reduced by changing the phase characteristic of the individual scatterers' returns at the point where the radar is located.

Space diversity technique aims to change the relative phases of scatterers by moving the position of the antenna. In this reduction technique, target return signals which are sampled at different radar positions are the outputs of the first stage. The first stage outputs are combined with diversity selection methods in the second stage. The diversity selection methods will produce better angle estimations using the spatial samples.

Although the frequency diversity is a prominent technique in the literature, space diversity is also investigated by researchers for the glint problem. Therefore, space or aspect diversity is examined in this chapter.

Firstly, the statistical properties of the target signal with space diversity will be analyzed. Formulation of the parameters will be made similar to the frequency diversity analysis.

- The autocorrelation function of the return signal with varying aspect angle will be found.
- The critical antenna movement will be found and its effect will be investigated.

After presenting the arguments related with aspect diversity, angle estimation performance of the technique will be analyzed.

- Simulations for different target and antenna movement configurations will be made. The performance of averaging algorithms will be discussed by inspecting the reduction results of each.
- Effects of space diversity parameters such as distance between samples and total movement of the antenna will be introduced.

Studying on the statistical properties and advantages of the frequency agility, several questions will be answered concerning the implementation of frequency diversity method. These questions can be summarized as:

- What numbers of spatial samples are needed?
- What is the effect of total antenna displacement?
- Which diversity selection method should be used for estimation?

In an effort to answer the above questions, space diversity simulations are carried out in MATLAB. The properties of a radar system which employs space diversity are presented by using the simulation outputs. Methods will be proposed for the effective usage of the space diversity.

5.2.1. Autocorrelation Function of Signals with Spatial Diversity

The target model for this derivation is the same with the one in the frequency agility chapter. Although the target geometry is the same, the target movement changes the nature of the model. The new target and radar geometry is given in Figure 5.15. In this model target is rotated from θ_1 to θ_2.

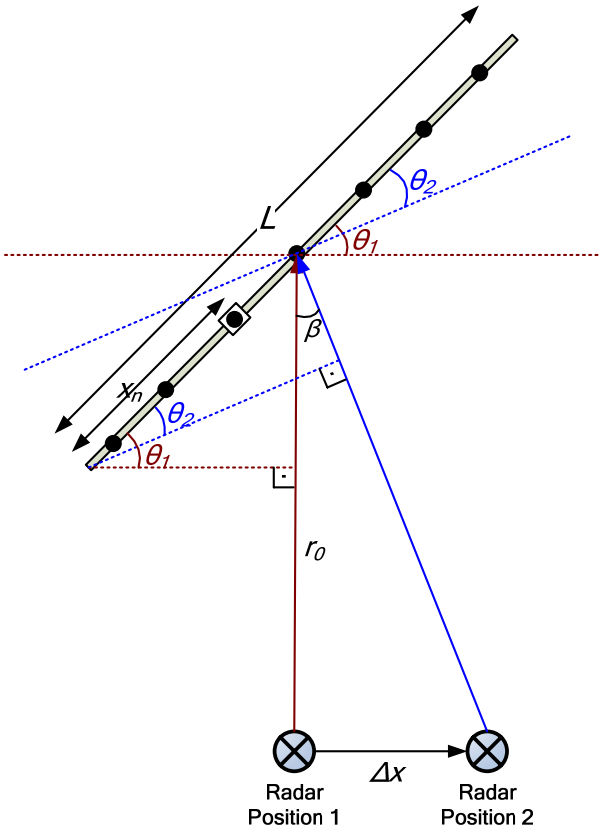

Figure 5.15 - Simple target geometry with aspect diversity

Let the return signal, $y(\theta)$, be

$$y(\theta) = \sum_n a_n e^{j(2\pi f \frac{2(r_0 + x_n * \sin(\theta))}{c} + \phi_n)} \tag{5.23}$$

The autocorrelation function can be formulated as:

$$R(\Delta\theta) = E\{y(\theta) * y^*(\theta + \Delta\theta)\} \tag{5.24}$$

$$R(\Delta\theta) = \sum_n \sum_m E\{a_n a_m\} e^{j2\pi f \frac{2x_n \sin(\theta)}{c}} e^{-j2\pi f \frac{2x_n \sin(\theta+\Delta\theta)}{c}} E\{e^{j(\phi_n - \phi_m)}\} \tag{5.25}$$

Similarly to the frequency diversity autocorrelation,

$$R(\Delta\theta) = {\mu_a}^2 \sum_n e^{j2\pi f \frac{2x_n}{c}(\sin(\theta) - \sin(\theta+\Delta\theta))} \tag{5.26}$$

At this point, if the target is assumed to be composed of infinite scatterers, the summation over the scatterers can be calculated as an integral over the distance from the middle of the target.

$$\int_{-L/2}^{L/2} e^{jxK} dx = \frac{2\sin\left(\frac{KL}{2}\right)}{K}, \qquad where\ K = 2\pi f \frac{2(\sin(\theta) - \sin(\theta + \Delta\theta))}{c} \tag{5.27}$$

The sinusoid terms in the above equation can be reformulated for small $\Delta\theta$ assumption as

$$\sin(\theta) - \sin(\theta + \Delta\theta) = -\sin(\Delta\theta)\cos(\theta) \tag{5.28}$$

Then the autocorrelation function reduces to

$$R(\Delta\theta) = {\mu_a}^2 \frac{\sin(2\pi f \frac{L\sin(\Delta\theta)\cos(\theta)}{c})}{2\pi f \frac{\sin(\Delta\theta)\cos(\theta)}{c}} \tag{5.29}$$

To summarize, an understandable expression of autocorrelation function is formulated for a simple line target. The autocorrelation function describes the nature of the target signal samples that are acquired at $\Delta\theta$ radian separations. The sinc structure in the expression is also similar to the frequency diversity analysis.

The correlation of the samples depends on the change in the aspect angle. For this reason, the angle change between the samples may affect the glint error totally. Next section of the chapter examines the autocorrelation function and makes the interpretation of the aspect angle change.

5.2.2. Critical Angle Change

The properties of the autocorrelation function are investigated to make effective reduction on glint. To begin with, the autocorrelation function of a 1m length target is given in Figure 5.16. Target orientation angle is 0^0 and radar center frequency is 10GHz.

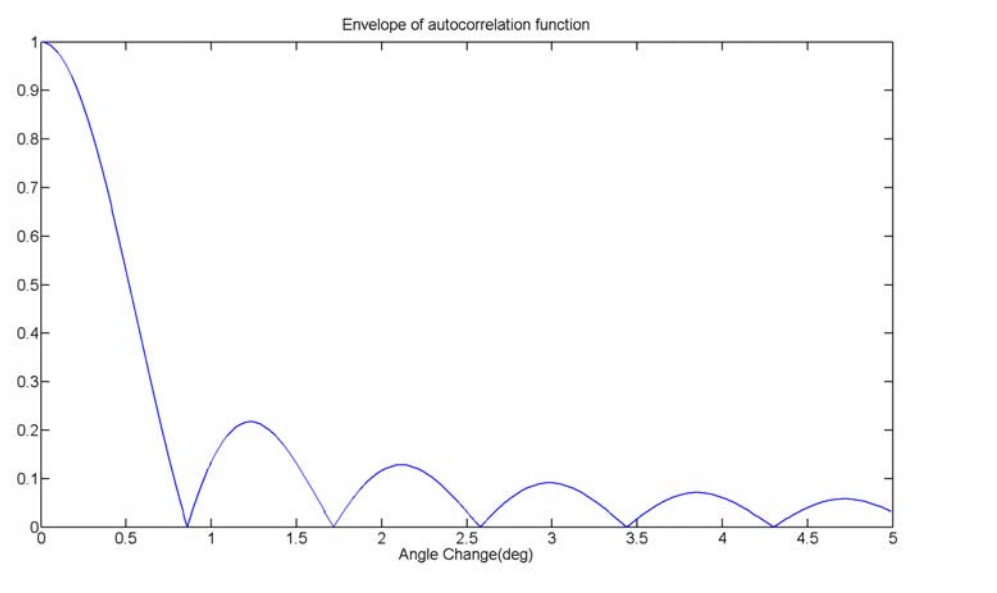

Figure 5.16 - Example of target signal's autocorrelation envelope for aspect changes

Figure 5.16 shows that samples for higher angle changes can be considered as uncorrelated. To determine a critical angle change, the first zero of the autocorrelation function can be used. The first zero occurs at $\Delta\theta_c$ which satisfies the below equation.

$$\sin(\Delta\theta_c) = \frac{c}{2fL\cos(\theta)} = \frac{c}{2fW}, \qquad where\ W = L\cos(\theta)\ is\ the\ target\ width \qquad (5.30)$$

5.2.3. Critical Antenna Movement

The critical angle change derived above can occur with the rotation of target itself. The radar system can benefit this rotation. However, the target rotation may not be sufficient to produce uncorrelated samples at the radar side. In this situation, the radar can move its antenna and may create an artificial angle change with its changing aspect with respect to the target.

Figure 5.15 also shows the new target geometry after Δx movement of the radar. The target orientation angle with respect to the radar is altering from θ_1 to θ_2 after shifting the antenna. Thus, the radar creates an artificial orientation angle change by the amount of $\theta_1 - \theta_2$. In this geometry the below equation can be introduced.

$$\Delta\theta = \theta_1 - \theta_2 = \beta \tag{5.31}$$

The angle β can now be considered as the critical angle change. Since the radar movement is too small compared to the target range, β can be expressed as

$$\sin(\beta) = \frac{\Delta \mathrm{x}}{r_0} \tag{5.32}$$

The radar movement which produces this critical angle change, β, can now be regarded as critical antenna movement. By using the above equations, the critical antenna movement, $\Delta \mathrm{x_c}$, can be expressed as

$$\Delta \mathrm{x_c} = \frac{r_0 c}{2fW} \tag{5.33}$$

5.2.4. Improvement with Spatial Diversity

An approximate improvement factor will be derived with similar approaches presented in frequency diversity. Probability of undercritical frequency jump is now can be considered as probability of undercritical space jump. In the context of space diversity, this probability can be expressed as

$$P_C = \frac{2\Delta x_c}{m_{SD}} = \frac{r_0 c}{m_{SD} f W} \tag{5.34}$$

where m_{SD} is the total antenna movement of space diversity system. Improvement factor can be expressed as

$$I = \sqrt{\frac{S_{FS}}{S_{SD}}} \tag{5.35}$$

S_{FS} : $Spectral\ density\ of\ glint\ with\ fixed\ space$

S_{SD} : $Spectral\ density\ of\ glint\ with\ space\ diversity$

S_{FS} corresponds to S_{FF} and S_{SD} corresponds to S_{FA} in the frequency agility case.

$$I^2 = \frac{1}{\frac{2B_G}{f_p} + P_C\left(1 - \frac{2B_G}{f_p}\right)} \tag{5.36}$$

Then we can assume $\left(1 - \frac{2B_G}{f_p}\right)$ as 1 since $\frac{2B_G}{f_p} \ll 1$. Thus, the improvement factor reduces to

$$I^2 = \frac{1}{\frac{1}{1/P_C} + \frac{1}{f_p/2B_G}} \tag{5.37}$$

Then similar to frequency agility case, the improvement factor for a system with space diversity can be approximated by

$$I^2 = \begin{cases} \frac{f_p}{2B_G} & , \quad if \quad f_p/2B_G \ll m_{SD}fW/r_0c \\ \frac{m_{SD}fW}{r_0c} & , \quad if \quad m_{SD}fW/r_0c \ll f_p/2B_G \end{cases} \tag{5.38}$$

Therefore the smallest of the two ratios above is the square of the improvement factor. Generally, the latter ratio is smaller and determines the improvement. To understand better a numerical example is given below. The example data and the ratios are

$$f_p = 5000Hz\,, B_G = 25Hz\,, f = 10GHz\,, W = 5m\,, r_0 = 1000m\,, m_{SD} = 20m \tag{5.39}$$

$$\frac{f_p}{2B_G} = 100 \quad and \quad \frac{m_{SD}fW}{r_0c} = 2.66 \tag{5.40}$$

The limiting factor in the example is the second ratio. Thus, the improvement factor depends on the total antenna movement for space diversity. In this case, improvement in glint reduction or target tracking is proportional to the square root of spatial shift in antenna position.

$$I \propto \sqrt{m_{SD}} \tag{5.41}$$

The second ratio can also be interpreted as higher spatial shift is needed for targets at higher ranges or the system should let the target to maneuver.

By using the above findings, an approximate improvement can be presented. A radar system can mitigate glint error by a factor of two with 25m displacement of antenna position for a target extending 5m in crossrange. The operating frequency of the radar is 10GHz and the target range is 1000m in this calculation.

Although this calculation is a rough estimate to improvement factor, it can still be a good point for starting the design of a radar system with space diversity.

5.2.5. Simulation Results of Spatial Diversity

The target model used in the simulations is the same with the model used in frequency diversity analyses. The center of the antennas used for direction finding is shifted with certain amounts in the simulation. Samples are acquired at each shifted antenna center point. Sample number in a space diversity system has great importance since the processing capacity and the antenna movement capabilities can be limited. Thus, the sample number effects are investigated in the simulation results. The total antenna movement can also be a limitation for the radar system. The artificial aspect change need in the space diversity should be satisfied by changing the center of the antennas. Therefore, the spatial shift is examined with the MATLAB simulations too.

5.2.5.1. Effect of Sample Number for a Fixed Spatial Shift

Sample number can be a critical factor in the implementation as mentioned above. Other than the processing burden to the system, physically extending the radar with desired amount may not be realizable. Therefore, the simulations are conducted for developing a notion on the selection of the sample number.

Table 5.5 - Simulation configuration of sample number analysis

	Target 1	**Target 2**
Target depth	5m	1m
Target width	5m	1m
Target angle	5deg	
Target range	1000m	
Random scatterers on target	10	
Shift in positions of the DF antennas	10m 40m	10m 40m
Maximum number of samples	20	
Center frequency of the radar	10GHz	
DF Method	Phase Monopulse	
Number of experiments	1000	

The simulation configuration shown in Table 5.5 is used for the examination of the sample number effect on glint error reduction for a fixed antenna movement. The spacing of the samples is linear from 0 to total antenna shift.

The simulation results for Target 1 which is a relatively larger target are given in Figure 5.17 and Figure 5.18. From the simulation configuration parameters, the critical spatial shift in radar position, Δx_c, results in 3m for Target 1. This means that 3m shift of the antenna can give uncorrelated samples of target return signal. Thus, both 10m and 40m total space used in diversity is sufficient.

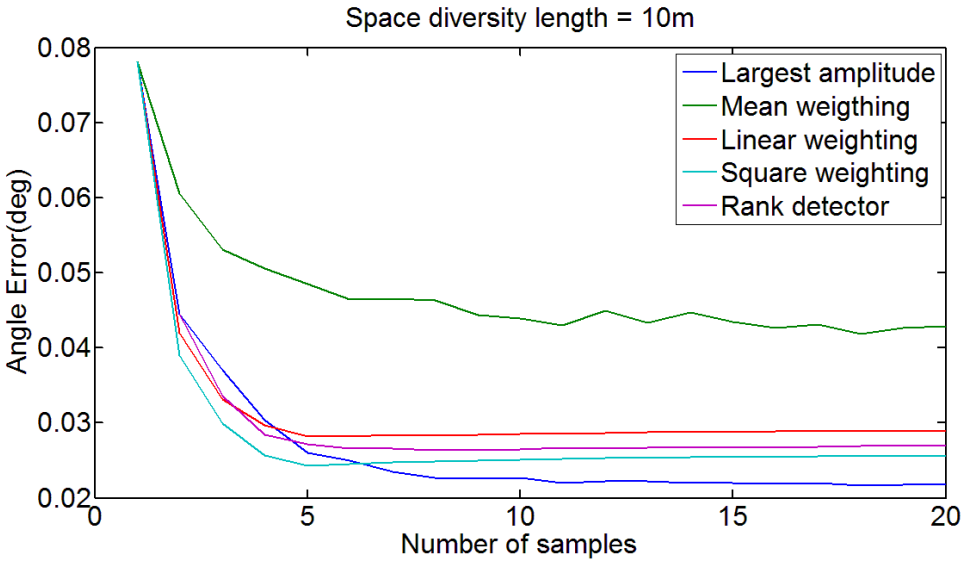

Figure 5.17 - Target 1 simulation results for 10m antenna movement

Firstly, the simulation results are shown for 10m total length for space diversity in Figure 5.17. The uncorrelated sample number which can be taken in this interval is 10/3 theoretically. As a result of this ratio, it is expected that 3 or 4 samples are enough for the diversity selection techniques to reduce the glint error.

The reduction results show that this is the case for all reduction techniques except for the largest amplitude selection method. However this method gives also steady error levels after 10 samples. The linear and square weighting and the rank detector methods give slightly increasing error for higher sample numbers since the samples become correlated. The largest amplitude selection method can give better results

for the correlated samples case which is also seen in the frequency agility analyses. However, taking unnecessarily extra samples in a limited space diversity length may be an undesirable situation for the radar considering the motion requirements. Consequently, one can speak of a tradeoff between the sample number and the achieved reduction level.

Secondly, the simulation results are shown for 40m total length for space diversity in Figure 5.18. The uncorrelated sample number which can be taken in this interval is 40/3 theoretically. Therefore, gathering more samples becomes more meaningful. By taking more uncorrelated samples, reduction methods have the opportunity to decrease the pointing angle error. The square weighting method is the best method for this configuration since the total movement interval is enough for the desired less correlated samples. However, the radar system should move the DF antennas 40m to improve the angle estimation of the target. This much movement is not realizable for most radars.

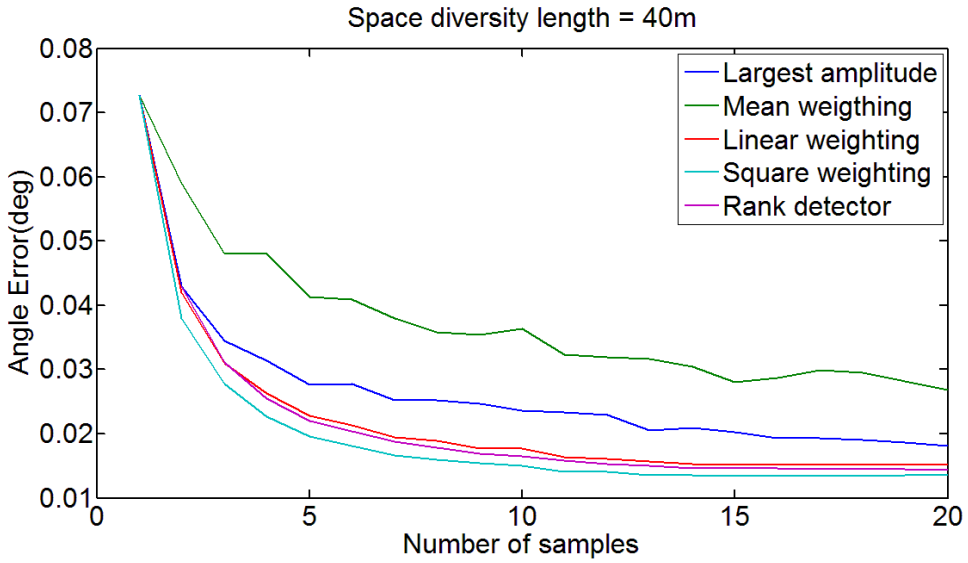

Figure 5.18 - Target 1 simulation results for 40m antenna movement

The simulation results for Target 2 are given in Figure 5.19 and Figure 5.20 in order to provide better understanding of the space diversity reduction technique mechanisms. Figure 5.19 and Figure 5.20 respectively show the reduction results of the space diversity with movement of 10m and 40m.

The critical antenna movement is 15m for this target and the current simulation environment. Thus, 10m movement case seen in Figure 5.19 is not enough for taking uncorrelated samples. This yields a weak square weighting method performance. The largest amplitude selection method is the best method for this insufficient antenna shift interval for all number of samples. The correlated samples make the output of the reduction process worse for other diversity selection methods.

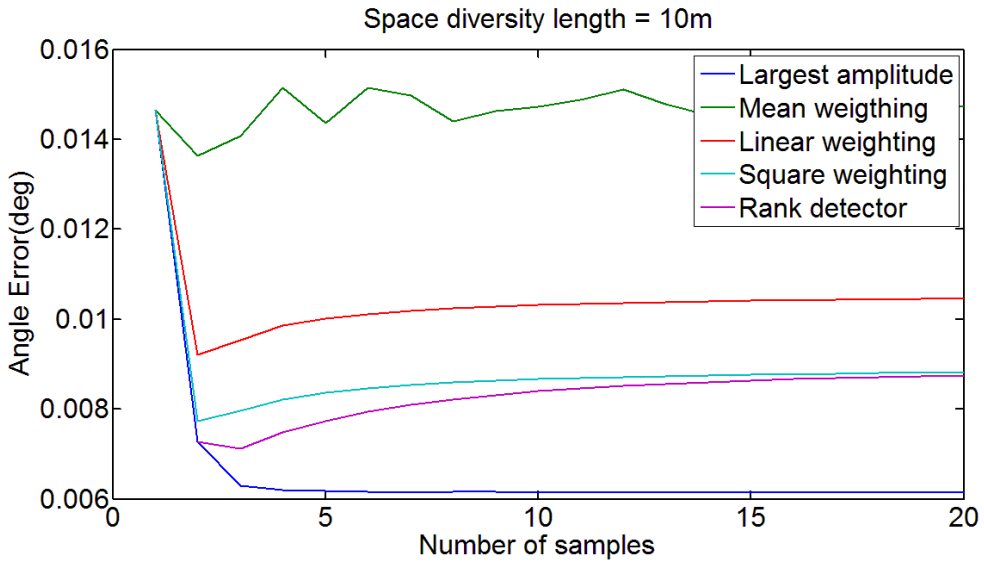

Figure 5.19 - Target 2 simulation results for 10m antenna movement

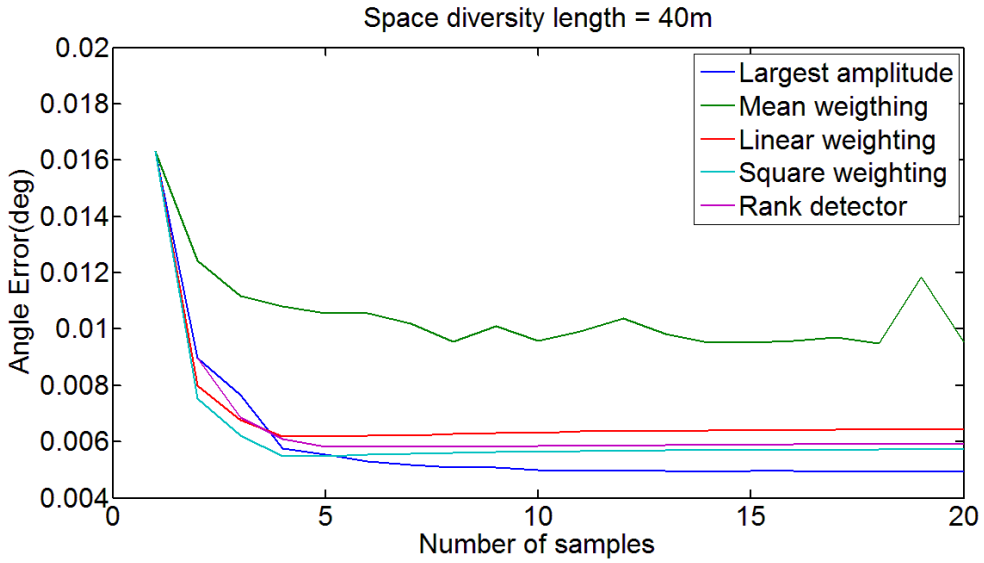

Figure 5.20 - Target 2 simulation results for 40m antenna movement

On the other hand, the case of 40m antenna movement is only enough for 3 or 4 uncorrelated samples. The return signals for higher number of samples become correlated. Therefore, a slight increase in error starts after 4 samples. Pointing error for the largest amplitude selection method stays steady for high sampled reduction scheme. As a result, it becomes the best diversity selection method.

5.2.5.2. Effect of Spatial Shift for a Fixed Number of Samples

In this section, the effect of the antenna movement interval will be examined. The performance of using space diversity in a radar system is investigated and the reduction results are presented. For better understanding of the simulation results, we can speak of a performance factor as mentioned in the frequency agility chapter. This performance factor is the ratio of the spacing of the samples in the movement interval and the critical spatial shift (Δx_c), i.e.

$$p_f = \frac{s_s}{\Delta x_c} \tag{5.42}$$

This performance factor may be a helpful factor in the design process of a radar system which employs space diversity for the reduction of angle errors due to the target glint. The interpretation of this factor is similar to the frequency diversity analysis. The intervals are given by using the reduction results of square weighting method.

1) If $p_f > 1$, total spatial shift cannot be used efficiently.
   - Spacing of the samples and number of samples may be increased to decrease p_f.
2) If $p_f < 1$, total spatial shift is unnecessarily much sampled.
   - Processing capacity of the system can be enhanced.
3) If $p_f \ll 1$, space diversity cannot reach the maximum improvement level.
   - Correlation of samples can be broken by increasing the spatial spacing. Number of samples will decrease in this case.

The second choice can be regarded as the most advantageous compared to others. The other intervals will suffer unsuccessful reduction levels. This factor and the

space diversity are analyzed with the simulation configuration presented below in Table 5.6.

Table 5.6 - Simulation configuration of antenna movement analysis

Target depth	10m
Target width	10m
Target angle	5deg
Target range	1000m
Random scatterers on target	5
Maximum shift in positions of the DF antennas	60m
Number of samples	15
Center frequency of the radar	10GHz
DF Antenna spacing	2.5mm
Number of experiments	1000

The simulation results are given for the square weighting and the largest amplitude selection methods, since both can be the best method for different spatial shift values. The improvement factor line which is normalized to the square weighting method corresponds to the theoretically reduced angle error. The performance factor line for the simulation parameters is also given to evaluate the reduction performance. These results are illustrated in Figure 5.21.

Figure 5.21 includes various situations related to the space diversity reduction performance. Before evaluating the results, it should be noted that the critical spatial shift for this simulation is 1.5m. The performance factor is increasing from 0.044 to 2.67 and spanning all three intervals mentioned above.

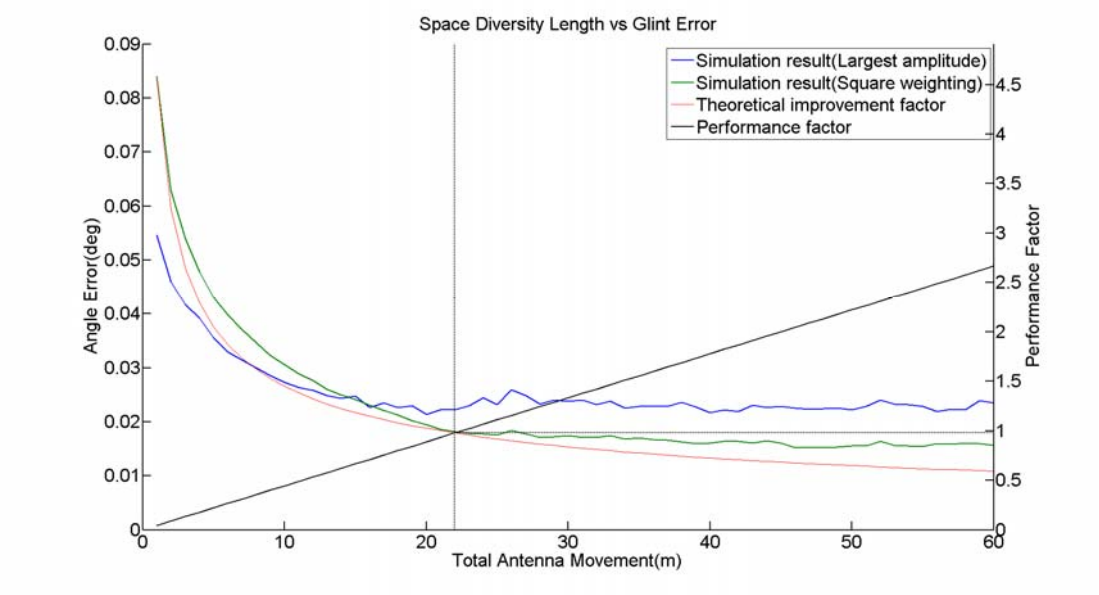

Figure 5.21 - Antenna movement effect on the reduction

The best possible diversity selection method is altering with increasing total spatial shifts. The correlation of the samples is strong when the total antenna movement is small. For this relatively strong correlation case, the largest amplitude selection is better than the square weighting. However, the square weighting method becomes superior with weakened sample correlation due to larger antenna movement values. Performance factor is also approaching to 1 while the best possible diversity selection method is changing from one to another. The square weighting method is better for $p_f > 1$.

The square weighting method and the improvement factor line should be investigated to understand how the performance factor is influencing the angle estimation error. The reduction output has a separation from the theoretical error line for $p_f < 1$ where the correlation of samples is relatively strong. The reduction results can reach the theoretically calculated error line for p_f values that are closer to one. Although uncorrelated samples are gathered for $p_f > 1$, reduction results cannot catch the expected reduction level. However, the reduction performance in this interval can be improved by taking more samples.

5.2.5.3. ISAR like Reduction Results

The space diversity aims to create an artificial aspect change to weaken the correlation of the samples. However, the radar may allow the target to rotate as in inverse synthetic aperture radar (ISAR) imagery and create this decorrelation itself.

The reduction procedure is repeated by allowing the target to maneuver. The rotating target model illustrated in Figure 5.22 is used for this purpose. The illustration is for only one scatterer, but the simulation contains a multi-point scatterer target.

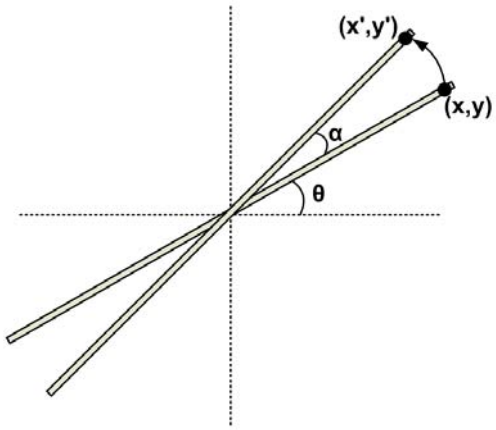

Figure 5.22 - Target geometry with rotating element

Rotation of the target will create new scatterer position with respect to the radar. It is assumed that target is rotating around the geometric center of the scatterers. As a result, new scatterer positions corresponding to "α" radian rotation are calculated with the below equations

$$x' = x * \cos(\alpha) - y * \sin(\alpha) \tag{5.43}$$

$$y' = x * \sin(\alpha) + y * \cos(\alpha) \tag{5.44}$$

The samples of the target return signal are taken at linearly spaced points between 0 and the total angle of rotation. The simulation configuration is given in Table 5.7 and the results are given in Figure 5.23.

Table 5.7 - Simulation configuration of ISAR like reduction

Target depth	10m
Target width	10m
Target angle	5deg
Target range	1000m
Random scatterers on target	5
Maximum rotation of target	60mrad
Number of samples	15
Center frequency of the radar	10GHz
DF Antenna spacing	2.5mm
Number of experiments	1000

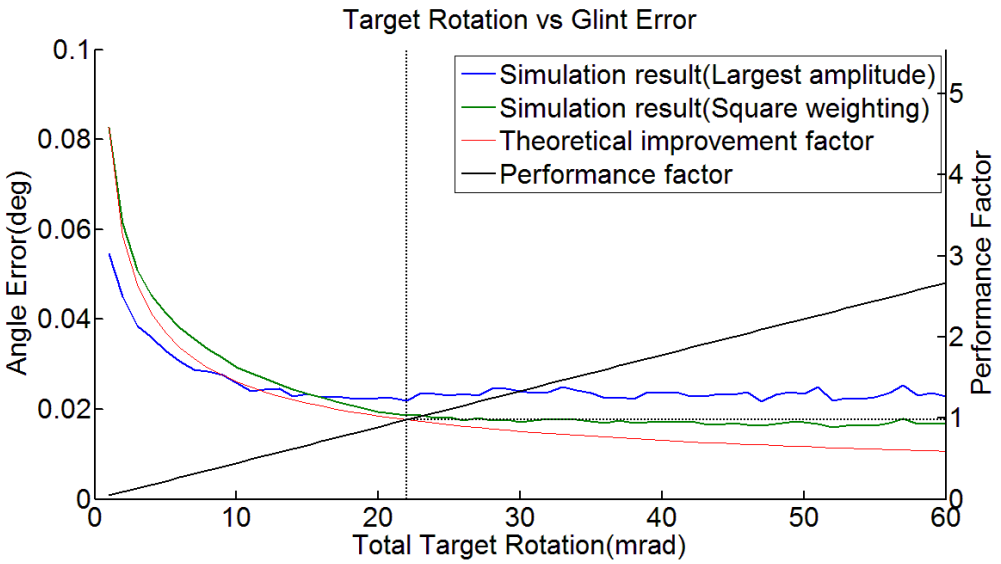

Figure 5.23 - Glint reduction with the usage of target maneuver

The critical angle change is 1.5mrad for this target and simulation parameters. The performance factor can be expressed as the ratio of rotation angle between consecutive samples (spacing of samples) and the critical angle change. This factor can be interpreted in the same manner presented in Section 5.2.5.2. The performance factor is increasing from 0.044 to 2.67. These values of performance factor cover all three intervals.

The reduction results and the performance factor effects are shown in Figure 5.23. The diversity selection method behavior is the same as the artificial spatial shift simulation. Performance factor which is closer to 1 makes the reduction performance reach the theoretical improved error line. Performance factor which is greater than 1 results in insufficient usage of the target rotation. Therefore, the output of the reduction algorithm stays steady for this interval.

The investigation and simulation on reduction by usage of target rotation as ISAR imagery shows that both artificial space diversity and ISAR like reduction are the same. The reduction results shown in Figure 5.21 and Figure 5.23 are very similar.

As a result of these discussions, the radar system can choose either the artificial space diversity reduction technique or ISAR like reduction technique. If the radar system deals with a high maneuvering target, it may be more suitable to choose the ISAR like reduction.

CHAPTER 6

CONCLUSION

In this thesis, mainly the performances of glint reduction techniques are investigated along with the effects of system parameters. For this reason, the main generating mechanisms of glint are discussed. By understanding the basics of the phenomenon, the characteristics of glint error are presented with analytical discussions.

The glint phenomenon is firstly demonstrated with the simple dumbbell model which can even generate glint errors that can go far beyond the physical extents of the target. After demonstration of simple glint generation scheme, general cases of target scattering interference are discussed.

Simple two target method put forward the scattering amplitude and phase dependences of glint error. For this reason, diversity methods are advised in literature for glint reduction purposes. As a result, frequency diversity and spatial diversity techniques are studied in detail in this thesis.

The analytical studies on glint error are also presented for different purposes. The basic properties of glint show that the glint error is only important under certain circumstances such as closer target ranges and larger target sizes. As a result, glint error can be treated as a problem for some specific systems like homing guided missiles.

To accomplish the objects of the thesis and to support the demonstration of glint properties, discrete modeling of glint is chosen. Simulations that integrate the echoes from each scattering elements of complex target are built up. In the

simulation model, the complex characteristics of each scattering elements are chosen randomly for general demonstrations.

The simulations of frequency diversity analyses use the same random complex scatterring for all frequencies. This approach in this model may not be realistic. However, the dependence of the complex scattering characteristic on frequency could not be found in the literature. Nevertheless, a dependence can be introduced in the simulations easily and the effects can be simply predicted by analyzing the correlation properties of the scattering characteristics. Similar discussions are also valid for spatial diversity.

The frequency diversity with the applied model is shown to be effective for glint error reduction. The frequency agility bandwidth is an increasing factor on reduction performance as both theoretically and experimentally demonstrated. Although the simulation results are only illustrated for 10GHz neighborhood, the correlation of the samples does not depend on frequency at all, but solely depends on the dimension of the target along the range direction. Therefore, the reduction of glint error with frequency diversity can be applied for all frequency bands.

The spatial diversity, on the other hand, depends on frequency band that is used for illumination. This property of the spatial diversity may be a limiting factor in utilization of the method for some systems. Nonetheless, the correlation requirements of both methods do not contradict with each other. As a result of this property, combination of the methods can be employed in radar systems.

Although, the diversity methods are shown to be effective on glint noise reduction by simulations and theory, the models for complex scattering characteristics of scattering elements are needed to be developed. Especially, hardware in the loop simulations may be promising for further understanding and analysis of glint errors with diversity techniques.

REFERENCES

1. M. Skolnik, “Introduction to Radar systems”, *McGraw-Hill,* 1980

2. M. Skolnik, “Radar Handbook”, *McGraw-Hill,* 2008

3. B. R. Mahafza, “Radar Systems Analysis and Design Using MATLAB”, *Chapman&Hall/CRC,* 2000

4. Wikipedia, “History of Radar” [Online]. Available at: http://en.wikipedia.org/wiki/History_of_radar

5. R. V. Ostravityanov and F. A. Basalov, translated by W. F. Barton and D. K. Barton, “Statistical theory of extended radar targets: a translation from the Russian of Statisticheskaya teoriya radiolokatsii protyazhennyz [sic] tselei”, *Artech House*, 1985

6. V. C. Chen, “Glint Errors Derived From the Partial Derivatives of the Echo Signal Phase for a Distributed Scatterer”, *Naval Research Laboratory*, May 1992

7. D. K. Barton and S. A. Leonov, “Radar Technology Encyclopedia”, *Artech House*, 1998

8. J. H. Dunn and D. D. Howard, “Phenomena of Scintillation Noise in Radar Tracking Systems”, *Proceedings of IRE*, vol. 47, pp. 855-863, May 1959

9. J. W. Wright, “Radar Glint-A Survey”, *Electromagnetics*, vol. 4, no. 2, pp. 205-227, January 1984

10. R. J. Sims and E. R. Graf, “The determination of glint for a complex radar target”, *Auburn University Guidance Systems Laboratory,* July 1969

11. R. H. Delano, “A Theory of Target Glint or Angular Scintillation in Radar Tracking”, *Proc. IRE*, vol. 41, pp. 1778-84, December 1953

12. N. M. Harter, “Development of Single-Channel Direction Finding Algorithm”, *Master’s Thesis, Virginia Polytechnic Institute and State University*, April 2007

13. B. Borden, “Diversity Methods in Phase Monopulse Tracking – A New Approach”, *IEEE Trans. On Aerospace and Electronic Systems*, vol. 27, no. 6, pp. 877-880, November 1991

14. B. Borden, “What is the Radar Tracking "Glint" Problem and can it be Solved?”, *Naval Air Warfare Center Weapons Division*, May 1993

15. G. A. Hewer, R. D. Martin and J. Zeh, “Robust Preprocessing for Kalman Filtering of Glint Noise”, *IEEE Trans. On Aerospace and Electronic Systems*, vol. 23, no. 1, pp. 120-128, January 1987

16. D. Chang and W. Wu, “Feedback Median Filter for Robust Preprocessing of Glint Noise”, *IEEE Trans. On Aerospace and Electronic Systems*, vol. 36, no. 4, pp. 1026-1035, October 2000

17. J. H. Dunn and D. D. Howard, “Radar Target Amplitude, Angle, and Doppler Scintillation from Analysis of the Echo Signal Propagating in Space”, *IEEE Trans. On Microwave Theory and Techniques*, vol. 16, no. 9, pp. 715-728, September 1968

18. I. W. Guest and C. K. Pauw, “Rank Detector Preprocessor for Glint Reduction in a Tracking Radar”, *IEEE Trans. On Aerospace and Electronic Systems*, vol. 29, no. 2, pp. 527-531, April 1993

19. G. Lind, “Reduction of radar tracking errors with frequency agility,” *IEEE Trans. Aerospace and Electronic Systems*, vol. AES-4, pp. 410-416, May 1968

20. G. Lind, “A Simple Approximate Formula for Glint Improvement with Frequency Agility”, *IEEE Trans. Aerospace and Electronic Systems*, vol. AES-8, pp. 854-855, November 1972

21. W. P. Birkemeir and N. D. Wallace, "Radar tracking accuracy improvement by means of pulse-to-pulse frequency modulation", *AIEE Trans. Communications and Electronics*, vol. 81, pp. 571-575, January 1963

22. R. J. Sims and E. R. Graf, “The reduction of radar glint by diversity techniques”, *IEEE Trans. Antennas and Propagation*, vol. AP-19, pp. 462-468, July 1971.

23. J. M. Loomis and E. R. Graf “Frequency-agility processing to reduce glint pointing error”, *IEEE Trans. Aerospace and Electronic Systems*, vol. AES-10, pp. 811-820, November 1974

24. R. B. Muchmore, “Aircraft Scintillation Spectra”, *IEEE Trans. Antennas and Propagation*, vol. AP-8, pp. 201-212, March 1960

25. L. Peters and F. C. Weimer, “Concerning the Assumption of Random Distribution of Scatterers as a Model of an Aircraft for Tracking Radars”, *IEEE Trans. Antennas and Propagation*, vol. AP-9, pp. 110-111, January 1961

26. N. S. Gubonin, “Fluctuations of the Phase Front of a Wave Reflected from a Complex Target”, *Radio Engineering and Electronic Physics*, vol. 10, pp. 718-725, May 1965

27. B. H. Borden and M. L. Mumford, “A Statistical Glint/Radar Cross Section Target Model”, *IEEE Trans. Aerospace and Electronic Systems*, vol. AES-19, pp. 781-785, September 1983

28. C. H. Cash and J. J. Jernigan, “N-Element Glint Simulator”, *US Patent 3,760,418*, September 1973

29. H. Yin and P. Huang, “Unification and Comparison Between Two Concepts of Radar Target Angular Glint”, *IEEE Trans. Aerospace and Electronic Systems*, vol. AES-31, pp. 778-783, April 1995

30. X. Shi, Y. Liu, X. Wang and C. Wang, “Angular glint of Aircraft Formation and Its Applications”, *Proceedings of the 2007 IEEE International Conference on Mechatronics and Automation*, pp. 1334-1339, August 2007

31. J. Chen, F. Yang, K. Zhang and J. Xu, “Angular glint modeling and simulation for complex targets”, *Proceedings of the 2008 IEEE International Conference on Microwave and Millimeter Wave Technology,* pp. 1899-1901, April 2008

32. Z. Zhen-yu, H. Zhi-yi, Z. Xin and L. Ye, “Practicable Research on Suppressing Angular Glint Base on the Target's RCS Weights”, *Proceedings of the 2010 IEEE 6th International Conference on Wireless Communications Networking and Mobile Computing,* pp. 1-5, September 2010